iScience

CellPress
OPEN ACCESS

Article

Intestinal microbiota modulates adrenomedullary response through Nod1 sensing in chromaffin cells

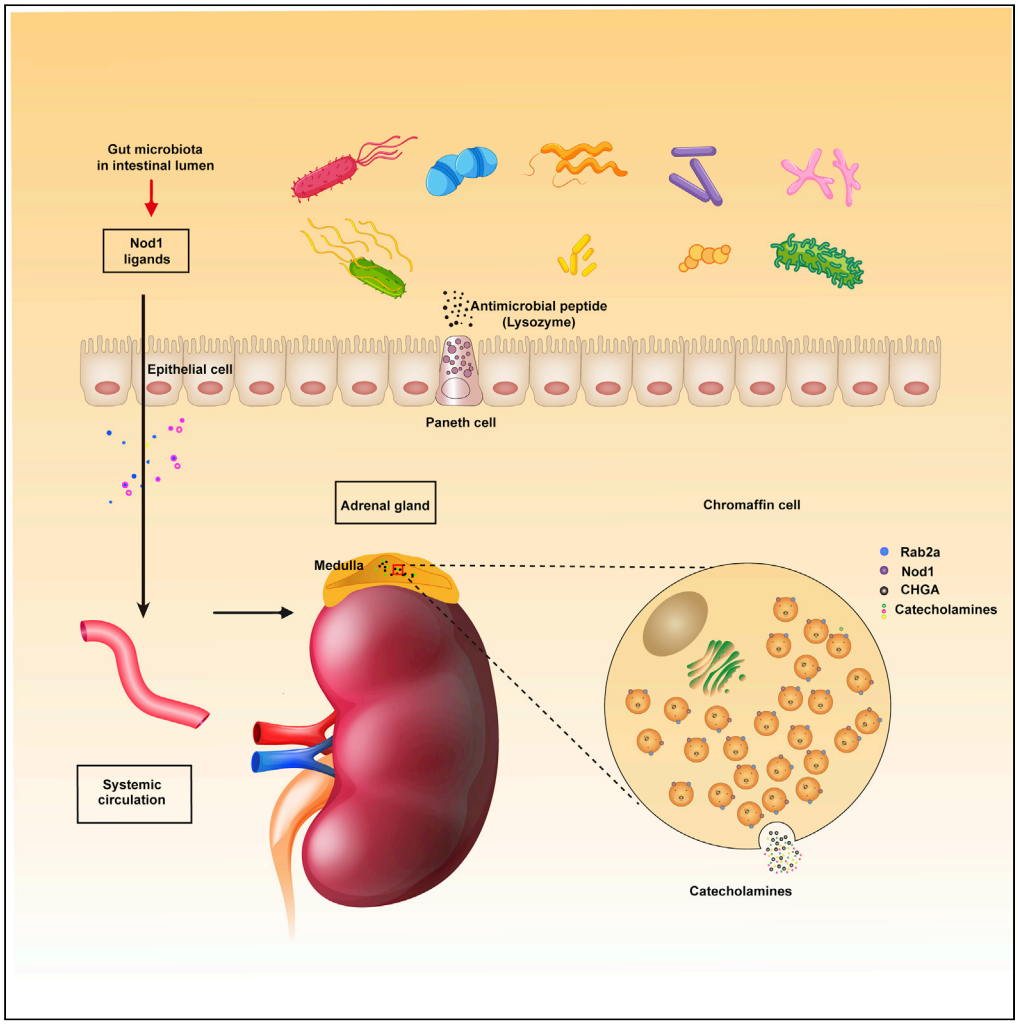

Chen Xiang, Peihua Chen, Qin Zhang, ..., Wenchun Xie, Jianyuan Sun, Zhihua Liu

jy.sun1@siat.ac.cn (J.S.)
zhihualiu@mail.tsinghua.edu.cn (Z.L.)

Highlights

Nod1 expressed in adrenal chromaffin cells senses intestinal bacteria

Bacterial Nod1 ligand promotes catecholamine storage and secretion

The microbiota-intestine-adrenal medulla axis modulates fight and flight response

Xiang et al., iScience 24, 102849
August 20, 2021
https://doi.org/10.1016/j.isci.2021.102849

iScience

CellPress
OPEN ACCESS

Article

Intestinal microbiota modulates adrenomedullary response through Nod1 sensing in chromaffin cells

Chen Xiang,[1,2,9] Peihua Chen,[2,3,4,9] Qin Zhang,[1] Yinghui Li,[1,2] Ying Pan,[1] Wenchun Xie,[5,6] Jianyuan Sun,[2,3,4,*] and Zhihua Liu[1,7,8,10,*]

SUMMARY

The intestinal microbiota closely interacts with the neuroendocrine system and exerts profound effects on host physiology. Here, we report that nucleotide-binding oligomerization domain 1 (Nod1) ligand derived from intestinal bacteria modulates catecholamine storage and secretion in mouse adrenal chromaffin cells. The cytosolic peptidoglycan receptor Nod1 is involved in chromogranin A (Chga) retention in dense core granules (DCGs) in chromaffin cells. Mechanistically, upon recognizing its ligand, Nod1 localizes to DCGs, and recruits Rab2a, which is critical for Chga and epinephrine retention in DCGs. Depletion of Nod1 ligand or deficiency of Nod1 leads to a profound defect in epinephrine storage in chromaffin cells and subsequently less secretion upon stimulation. The intestine-adrenal medulla cross talk bridged by Nod1 ligand modulates adrenal medullary responses during the immobilization-induced stress response in mice. Thus, our study uncovers a mechanism by which intestinal microbes modulate epinephrine secretion in response to stress, which may provide further understanding of the gut-brain axis.

INTRODUCTION

Accumulating evidence has shown that microbes residing in the intestine are deeply intertwined with diverse aspects of host physiology, ranging from metabolism, immune development, and immune responses to neuronal development and activity (Blander et al., 2017; Fung et al., 2017; Nicholson et al., 2012; Rooks and Garrett, 2016). It is emerging that the neuroendocrine system closely interacts with the gut microbiota (Farzi et al., 2018). Gut dysbiosis leads to profound alterations in neuroendocrine, neurochemical, and behavioral parameters (Crumeyrolle-Arias et al., 2014; Foster and McVey Neufeld, 2013; Rogers et al., 2016; Zheng et al., 2016). Uncovering the molecular mechanisms underlying such cross talk between microbes and the neuroendocrine system is of importance to understand the role of the microbiota in host health and disease.

The neuroendocrine system controls vital processes in response to acute or chronic stress. The sympatho-adrenal-medullary (SAM) and hypothalamic-pituitary-adrenocortical (HPA) axes are the primary systems involved in the stress response. It has been recognized that the intestinal microbiota impacts stress responses. Absence of microbiota (germ-free [GF] status) or depletion of microbes by antibiotics in rodents leads to exaggerated activation of the HPA axis associated with elevated adrenocorticotrophic hormone and corticosterone levels in response to stress, accompanied with reduced anxiety (Sudo et al., 2004; Zheng et al., 2016; Diaz Heijtz et al., 2011; Huo et al., 2017). Colonization by microbiota has been shown to regulate the expression of critical HPA axis genes in hippocampus and modulate hippocampal serotonin concentration, which also affects HPA activation (Luo et al., 2018; Farzi et al., 2015; Shanks et al., 1995; Clarke et al., 2013). Innate immune receptors are one of the mechanisms underlying the effect of microbiota on the HPA axis (Liu et al., 2014; Zacharowski et al., 2006). In comparison, the effect of intestinal microbiota on the SAM pathway has not been extensively investigated. One previous study found that the absence of gut microbial colonization selectively impaired catecholamine response to hypoglycemic stress in mice (Giri et al., 2019); however, the molecular mechanism was not identified.

Nucleotide-binding oligomerization domain 1 (Nod1), together with Nod2, as classic pattern recognition receptors, play a key role in mediating the microbe-host cross talk, including lymphoid tissue genesis

[1]Key Laboratory of Infection and Immunity, Institute of Biophysics, Chinese Academy of Sciences, Beijing 100101, China

[2]University of Chinese Academy of Sciences, Beijing 100049, China

[3]The Brain Cognition and Brain Disease Institute, Shenzhen Institutes of Advanced Technology, CAS; Shenzhen-Hong Kong Institute of Brain Science-Shenzhen Fundamental Research Institutions, Shenzhen 518055, China

[4]State Key Laboratory of Brain and Cognitive Sciences, Institute of Biophysics, CAS, Beijing, 100101, China

[5]Key Laboratory of Interdisciplinary Research, Institute of Biophysics, Chinese Academy of Sciences, Beijing 100101, China

[6]Guang Dong Bio-healtech Advanced Co., Ltd., Foshan, 528000, P. R. China

[7]Institute for Immunology, Tsinghua University, Beijing 100084, China

[8]Tsinghua-Peking Center for Life Sciences, Beijing 100084, China

[9]These authors contributed equally

[10]Lead contact

*Correspondence: jy.sun1@siat.ac.cn (J.S.), zhihualiu@mail.tsinghua.edu.cn (Z.L.)

https://doi.org/10.1016/j.isci.2021.102849

(Bouskra et al., 2008), Paneth cell function in the intestine (Zhang et al., 2015), neutrophil priming (Clarke et al., 2010), hematopoiesis (Iwamura et al., 2017), and 5-hydroxytryptamine (5-HT) signaling (Pusceddu et al., 2019). Our previous studies have found specific roles of Nod1 and Nod2 in modulating the intracellular membrane trafficking events of dense core granules (DCGs) in islet beta cells and intestinal Paneth cells (Zhang et al., 2015, 2019), indicating that DCG-mediated secretion could be subjected to regulation from commensal bacteria.

In this study, we found that Nod1 was highly expressed in adrenal chromaffin cells. Intestinal microbe-derived Nod1 ligand modulated hormone secretion in chromaffin cells. Mechanistically, we found that Nod1 localized to DCGs and recruited Rab2a onto DCGs, which subsequently affected Chga retention in DCGs. Microbe sensing through Nod1 was required for efficient storage and secretion of epinephrine in adrenal chromaffin cells. Finally, specific deficiency of Nod1 in chromaffin cells impaired epinephrine secretion during immobilization stress in mice. Collectively, our results identify a new microbe-host cross talk pathway, in which adrenal chromaffin cells sense microbial Nod1 ligand released from commensal bacteria by intestinal lysozyme to optimize epinephrine secretion during immobilization stress.

RESULTS

Nod1 expressed in adrenal chromaffin cells modulates epinephrine secretion

Immunohistochemical (IHC) staining of adrenal gland from wild-type (WT) mice detected Nod1 expression specifically in the medulla, but not in the cortex region, whereas *Nod1* deficiency abolished staining in the medulla region (Figure 1A). Quantitative polymerase chain reaction in WT tissues showed that *Nod1* mRNA was highly enriched in medulla but very low in the cortex (Figure 1B). The overall level of *Nod1* mRNA in adrenal glands was relatively low, probably because the medulla is not the major part of the adrenal gland. Notably, *Nod1* mRNA and protein levels in the medulla were almost comparable to those in spleen, which is known to express Nod1 at a high level (Figures 1B, S1A, and S1B), as previously reported (Inohara et al., 1999).

We next sought to understand the biological function of Nod1 in adrenal chromaffin cells. Adrenal chromaffin cells are classic neuroendocrine cells, which secrete catecholamines upon receiving stimulation from sympathetic nerves (Fenwick et al., 1982; Sala et al., 2008). Epinephrine is the major form of catecholamine present in adrenal chromaffin cells. Catecholamine secretion can be monitored in a real-time manner using specific probes (Muller et al., 2014; Wang et al., 2018). A G protein-coupled receptor (GPCR) activation-based NE ($GRAB_{NE}$) probe, based on an $\alpha 2$ adrenergic receptor, has been developed for *in vivo* and *in vitro* measurement of epinephrine or norepinephrine dynamics (Feng et al., 2019). The $GRAB_{NE}$ sensor was constructed by inserting a circularly permutated enhanced green fluorescent protein (eGFP) between the fifth and sixth transmembrane domains of the $\alpha 2$ adrenergic receptor. When epinephrine or norepinephrine binds to the extracellular domain of the $GRAB_{NE}$ sensor, a conformational change occurs between the fifth and sixth transmembrane domains to activate the green fluorescence of eGFP. Thus, when $GRAB_{NE}$ sensor is expressed on the cell surface, its fluorescence reflects the level of epinephrine/norepinephrine in the extracellular environment (Figure S1C). We employed the $GRAB_{NE}$ assay to monitor the secretion activity of chromaffin cell upon stimulation. *Ex vivo* cultured chromaffin cells were transfected with the $GRAB_{NE}$-encoding plasmid and subjected to K^+ treatment to induce secretion. The resulting fluorescence flux was recorded, and the changes of green fluorescence intensities ($\Delta F/F0$) were calculated to reflect the epinephrine (norepinephrine) level (Figures S1D and S1E). As originally published (Feng et al., 2019), the $GRAB_{NE}$ plasmid also encodes a plasma membrane-targeted mCherry following the coding sequence of $GRAB_{NE}$ using an internal ribosome entry site (IRES) sequence. Translation of this mCherry reporter through an IRES sequence is used to monitor possible photobleaching during the experimentation. No photobleaching was apparent during our experiments (Figures S1D and S1E).

We employed the $GRAB_{NE}$ method to evaluate whether Nod1 or Nod1 ligand could affect the secretion of epinephrine (and, to a lesser extent, norepinephrine) from *ex vivo* cultured chromaffin cells. iE-DAP was used as the Nod1 agonist. A concentration of 1 μg/mL iE-DAP was chosen because we previously showed that it could restore the Nod1 ligand activity of sera from GF mice to a level comparable to that in specific pathogen-free (SPF) mice (Stojanovic and Trajkovski, 2019). iE-Lys was used as the negative control for iE-DAP. In addition, lipopolysaccharides (LPS), the TLR4 ligand, and muramyl dipeptide (MDP), the Nod2 ligand, were included. Transient transfection of $GRAB_{NE}$ inevitably resulted in different expression level,

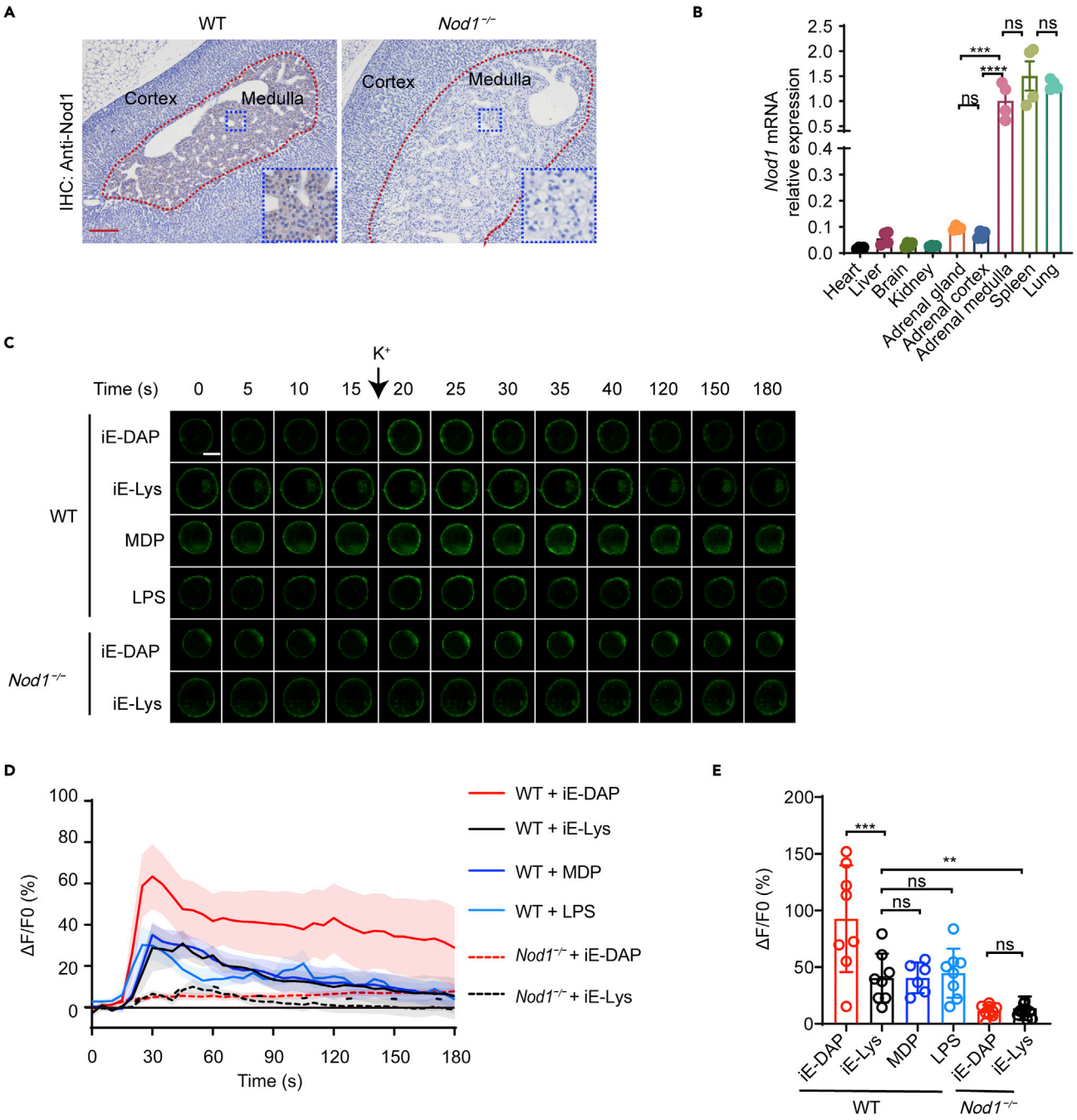

Figure 1. Adrenal chromaffin cells express Nod1 and sense Nod1 ligand

(A) Immunohistochemical (IHC) staining of Nod1 in paraffin sections of adrenal gland from wild-type (WT) and *Nod1*$^{-/-}$ mice. Medullary regions are outlined with a red dashed line. Blue boxed areas are shown at higher magnification (4 times enlarged) in the insets in the bottom right corner.

(B) Relative *Nod1* mRNA levels in indicated tissues determined by quantitative PCR. The *Gapdh* mRNA level was used for normalization (n = 4 mice).

(C) Representative images of green fluorescence of $GRAB_{NE}$ in transfected chromaffin cells during the course of treatment with K^+ solution (90 mM) to trigger secretion.

(D) The recorded relative fluorescence changes of $GRAB_{NE}$ over the time course of the experiment (ΔF/F0) (n = 6–11 cells from 5 to 8 mice).

(E) The maximum peak of ΔF/F0 in the different treatment groups from (D).

Scale bars: 120 μm (A), 5 μm (C). Each symbol represents an individual mouse in (B) or an individual cell in (E). Summary plots show all data points with mean and s.e.m (B and E). The line connects means of fluorescence change over the time course with ribbons indicating ±s.e.m. (D). Statistically significant differences were determined using one-way ANOVA followed by Tukey's post hoc test (B, E). ns, not significant, *p < 0.05, **p < 0.01, ***p < 0.001. Experiments were repeated at least three times (A, B, C).

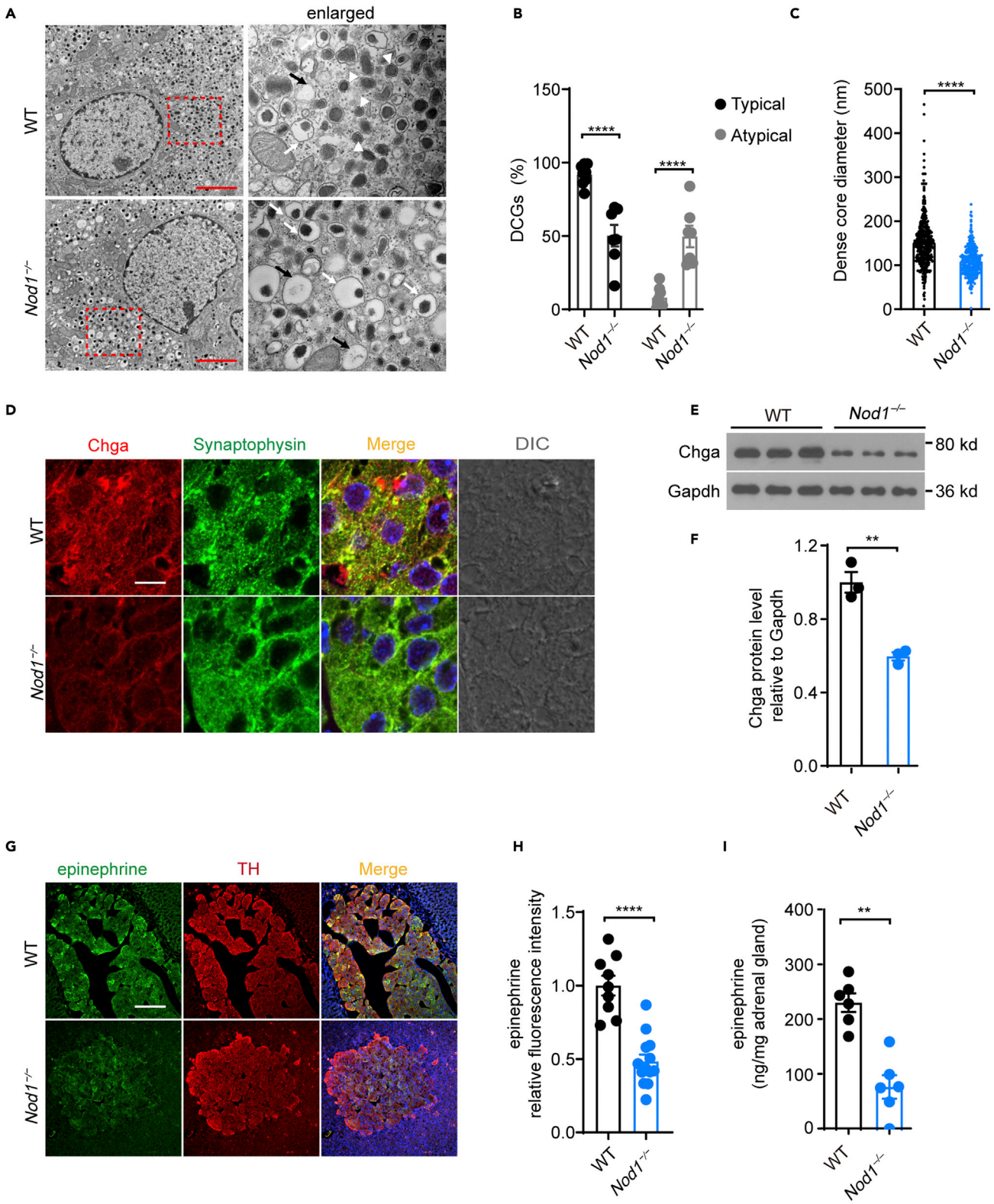

Figure 2. Nod1 affects the amount of Chga and epinephrine in DCGs

(A) Electron microscopy images of epinephrine-storing cells from WT and *Nod1*$^{-/-}$ mice. Boxed areas are shown at higher magnification (3 times enlarged) in the panels on the right. White arrowheads indicate type 1 DCGs, white arrows indicate type 2 DCGs and black arrows indicate type 3 DCGs.

Figure 2. *Continued*

(B) Quantification of typical (type 1) vs atypical (type 2, 3) DCGs in medullas from WT (n = 10 cells) and *Nod1*$^{-/-}$ (n = 8 cells) mice.
(C) Quantification of dense core diameters in type1 and type 2 DCGs present in chromaffin cells in WT (n = 502 DCGs) and *Nod1*$^{-/-}$ (n = 334 DCGs) mice.
(D) Immunostaining and confocal imaging of synaptophysin (green) and Chga (red) in paraffin sections of adrenal glands from WT and *Nod1*$^{-/-}$ mice.
(E) Representative immunoblots of Chga in the dissected adrenal medullas from WT (n = 3) and *Nod1*$^{-/-}$ (n = 3) mice. Gapdh was used as a loading control.
(F) Relative level of Chga protein compared to Gapdh in isolated adrenal medullas, analyzed by immunoblotting, and quantified by densitometry.
(G) Immunostaining and confocal imaging of epinephrine (green) and TH (red) in paraffin sections of adrenal glands from WT and *Nod1*$^{-/-}$ mice.
(H) Quantification of relative epinephrine fluorescence in the images related to (G).
(I) The amount of epinephrine in adrenal glands in WT and *Nod1*$^{-/-}$ mice.
Scale bars, 2 μm (A), 10 μm (D), 100 μm (G). Statistically significant differences were determined using the student's *t*-test (B, C, F, H, I). $^{**}p < 0.01$, $^{***}p < 0.001$ and $^{****}p < 0.0001$. Each symbol represents an individual mouse (F, I). Mean and s.e.m. are indicated (B, C, F, H, I). Data (D-G) are representative of three independent experiments.

indicated by different basal level of $GRAB_{NE}$ fluorescence. However, we found that the max F/F0 did not correlate with basal level of $GRAB_{NE}$ fluorescence (Figure S1F). Furthermore, analysis of the distribution of basal level of $GRAB_{NE}$ fluorescence suggested that treatment with different compounds did not overtly affect basal level of $GRAB_{NE}$ fluorescence in transfected primary chromaffin cells and PC-12 cells (Figures S1G–S1I), a cell line derived from a pheochromocytoma of the rat adrenal medulla (Greene and Tischler, 1976).

As expected, a green fluorescence flux was induced on the plasma membrane of the chromaffin cells upon K^+ stimulation (Figure 1C). Notably, K^+ induced comparable green fluorescence flux in WT cells treated with iE-Lys, LPS, and MDP (Figures 1C and 1D), while a much stronger fluorescence flux was observed in WT cells treated with iE-DAP (Figures 1C and 1D). The maximum changes of fluorescence intensity (Max ΔF/F0) were significantly increased in iE-DAP-treated WT chromaffin cells compared with WT cells treated with iE-Lys, MDP, or LPS (Figure 1E).

Chromaffin cells from *Nod1*$^{-/-}$ mice did not respond to K^+ stimulation as robustly as cells from WT mice (the iE-Lys-treated groups in Figures 1C–1E). iE-DAP treatment did not enhance the fluorescence flux in *Nod1*$^{-/-}$ cells as it did in cells from WT mice (Figures 1C–1E). Thus, Nod1 agonist can boost catecholamine secretion from chromaffin cells in a Nod1-dependent manner.

Nod1 deficiency reduces the abundance of Chga and epinephrine in adrenal chromaffin cells

Adrenal chromaffin cells store epinephrine (norepinephrine) in DCGs. We employed transmission electron microscopy (TEM) to analyze the morphology of DCGs. DCG morphology differs greatly between epinephrine-storing and norepinephrine-storing cells under the fixation condition we used (Figure S2A). We analyzed epinephrine-storing cells in our study. In epinephrine-storing cells, three types of vesicles were present: (1) a thin halo with a dense core (indicated by white arrowheads in Figure 2A), (2) a swollen halo with a dense core structure (indicated by white arrows in Figure 2A), and (3) a swollen halo with no noticeable dense core (indicated by black arrows in Figure 2A). Most of the vesicles in WT chromaffin cells had a dense core surrounded by a thin halo (type 1). A few vesicles in WT cells had dense cores that appeared less compact (type 2); these might represent DCGs undergoing maturation. In comparison, *Nod1*$^{-/-}$ chromaffin cells were predominantly filled with enlarged vesicles, either with less compact cores (type 2, Figure 2A) or without dense cores (type 3, Figure 2A). We quantified the numbers of typical DCGs (type 1) and atypical ones (types 2 and 3) in chromaffin cells from WT and *Nod1*$^{-/-}$ mice (Figure 2B). Around 40% of vesicles in chromaffin cells from *Nod1*$^{-/-}$ mice appeared atypical, compared to 10% in WT cells. Furthermore, among the DCGs with dense cores (type 1 and type 2), the diameters of the cores were smaller in chromaffin cells from *Nod1*$^{-/-}$ mice (Figure 2C). These data indicate that *Nod1* deficiency leads to abnormalities in DCG formation in chromaffin cells.

Chga plays a key role in the formation of DCGs (Kim et al., 2001). We probed for Chga in adrenal medulla of WT and *Nod1*$^{-/-}$ mice and found that the Chga immunofluorescence signal was markedly reduced in *Nod1*$^{-/-}$ medullas compared with WT medullas (Figures 2D and S2B). Although TEM showed enlarged vesicles in chromaffin cells from *Nod1*$^{-/-}$ mice (Figure 2D), the immunofluorescence signal of the DCG membrane protein synaptophysin (Figure 2D) appeared largely normal in confocal images of chromaffin cells from *Nod1*$^{-/-}$ mice. The resolution of confocal imaging of fixed paraffin-embedded tissue might not be sufficient to detect small alternations in vesicle size. To quantify Chga protein, we performed immunoblotting on isolated adrenal medullas from WT and *Nod1*$^{-/-}$ mice. Loss of Nod1 markedly reduced the amount

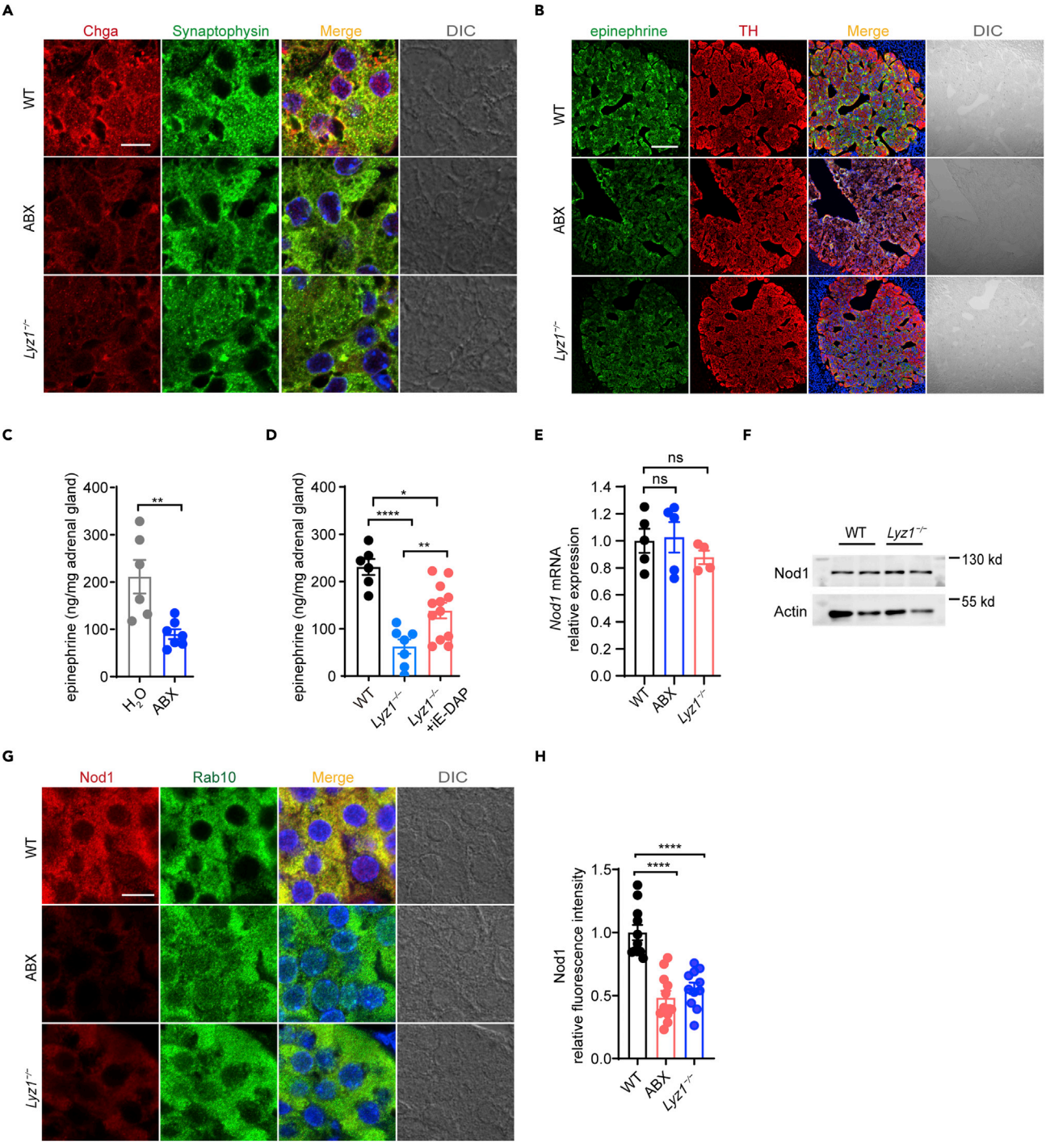

Figure 3. Microbe-derived Nod1 ligand modulates the amount of Chga and epinephrine in chromaffin cells

(A) Immunostaining and confocal imaging of Chga (red) and synaptophysin (green) in adrenomedullary tissue sections from WT, ABX, and *Lyz1*$^{-/-}$ mice.

(B) Immunostaining and confocal imaging of epinephrine (green) and TH (red) in paraffin sections of adrenal glands from the indicated mice.

(C and D) The epinephrine content in adrenal glands from mice treated with H_2O (vehicle, n = 6) or antibiotic cocktail (ABX, n = 7), as well as in adrenal glands from WT (n = 6), *Lyz1*$^{-/-}$ (n = 5), and *Lyz1*$^{-/-}$ orally supplemented with iE-DAP (n = 12) mice.

(E) The relative level of *Nod1* mRNA in isolated medullary region from the indicated mice (WT, n = 5; ABX, n = 5; *Lyz1*$^{-/-}$, n = 4) determined by quantitative PCR.

(F) Immunoblotting of Nod1 in isolated medullary regions from the indicated mice. Actin was used as a loading control.

Figure 3. *Continued*

(G) Immunostaining and confocal imaging of Nod1 (red) and Rab10 (green) in adrenomedullary tissue sections from the indicated mice.

(H) Quantification of relative Nod1 fluorescence in the images related to (G).

Scale bars, 10 μm (A, B, and G). Statistically significant differences were determined using the student's *t*-test (C) and one-way ANOVA (D and E). $^{**}p < 0.01$ and $^{****}p < 0.0001$. Each symbol represents an individual mouse. Mean and s.e.m. are indicated (C, D, E, and H). Data (A, B, F, G, and H) are representative of three independent experiments.

of Chga protein (Figures 2E and 2F). Meanwhile, *Chga, Chgb, Synaptotagmin I, and Carboxypeptidase E* mRNA levels were comparable in isolated adrenal medullas from WT and *Nod1*$^{-/-}$ mice (Figures S2C–S2F). In addition, mRNA levels of genes involved in epinephrine synthesis and 5-HT recycling were similar in WT and *Nod1*$^{-/-}$ mice (Figures S2G–S2I).

Chga is critical for epinephrine condensation in DCGs (Pasqua et al., 2016). We used an antibody to probe for epinephrine in adrenal medullas and found that the anti-epinephrine immunofluorescence was weaker in medullas from *Nod1*$^{-/-}$ mice compared with medullas from WT mice (Figures 2G and 2H). Tyrosine hydroxylase (TH) was stained to mark chromaffin cells (Figure 2G). We further quantified the amount of epinephrine in adrenal glands and found that *Nod1* deficiency markedly reduced the abundance of epinephrine (Figure 2I). Thus, deficiency of Nod1 leads to reduced levels of Chga and epinephrine in DCGs.

Microbial Nod1 ligand regulates the abundance of Chga and epinephrine in DCGs

Nod1 ligand derived from intestinal microbes is known to get into the circulation and modulate a range of biological activities in a Nod1-dependent manner (Bouskra et al., 2008; Chan et al., 2017; Zhang et al., 2019; Hergott et al., 2016; Iwamura et al., 2017). Here, we suspected that Nod1 ligand from intestinal microbes might be involved in regulating Nod1 activity in adrenal chromaffin cells. Treatment with antibiotics has been used to deplete microbial ligands in the circulation (Clarke et al., 2010; Bird, 2010; Arentsen et al., 2017; Hergott et al., 2016). We found that treatment of mice with a cocktail of antibiotics (ABX) significantly reduced the bacterial load and diminished the Chga staining in chromaffin cells (Figures 3A, S3A, and S3B). Since oral gavage could be stressful, we subjected a group of mice to the same oral gavage procedure with H_2O. Oral gavage itself did not affect Chga staining in chromaffin cells (Figure S3B). We previously reported that the presence of circulating Nod1 ligand depends on lysozyme in the intestinal lumen, and deficiency of Lyz1 in mice leads to reduced level of microbial Nod1 ligand in the circulation (Zhang et al., 2019). We immunostained Chga in adrenal glands in *Lyz1*$^{-/-}$ mice and found that the Chga signal was diminished in chromaffin cells (Figures 3A and S3C).

We further determined whether the amount of epinephrine was affected in mice lacking Nod1 ligand. Immunofluorescence staining detected a marked reduction of epinephrine in TH^{+} cells in adrenal glands in ABX or *Lyz1*$^{-/-}$ mice compared with WT mice (Figures 3B and S3D). Quantification confirmed that this reduction was highly significant in ABX or *Lyz1*$^{-/-}$ mice compared with control groups (Figures 3C and 3D). Of note, the overall structure and the relative ratio between medulla to whole adrenal gland was not altered in *Lyz1*$^{-/-}$ mice (Figures S3E–S3J). To further determine whether Nod1 ligand was involved in modulating the amount of adrenal epinephrine, we orally supplemented *Lyz1*$^{-/-}$ mice with iE-DAP. The supplementation partially restored the level of epinephrine in *Lyz1*$^{-/-}$ mice (Figure 3D). Previously, oligopeptide transporters encoded by SLC15A3 and SLC15A4 were reported to be responsible for transporting small peptidoglycan (PGN) fragments into macrophages (Nakamura et al., 2014). Here, we found that both transporters were expressed in adrenal medulla (Figures S3K and S3L). We suspected that such transporters might be responsible for transporting microbial Nod1 ligand into chromaffin cells.

To determine how Nod1 ligand and Nod1 receptor were involved in Chga and epinephrine storage in DCGs, we first determined whether ABX treatment or *Lyz1* deficiency might affect the expression of Nod1 in adrenal gland. *Nod1* mRNA levels were comparable among WT, ABX-treated, and *Lyz1*$^{-/-}$ mice (Figure 3E). Immunoblotting showed comparable levels of Nod1 in isolated adrenomedullas from WT and *Lyz1*$^{-/-}$ mice (Figure 3F), which was confirmed by IHC in adrenal glands (Figures S3M and S3N). We determined the cellular localization of Nod1 in adrenal glands from WT, ABX-treated, and *Lyz1*$^{-/-}$ mice. We used Rab10 to mark the DCGs (Figure 3G). Rab10 colocalized with Chga on DCGs in WT chromaffin cells (Figure S3O), consistent with the previous publication indicating Rab10 localization on DCGs in intestinal Paneth cell (Zhang et al., 2015). Nod1 colocalized with Rab10 in the adrenomedullary region in WT mice, indicating the recruitment of Nod1 onto DCGs (Figure 3G). However, the recruitment of

Nod1 onto DCGs was significantly reduced in ABX-treated or *Lyz1*$^{-/-}$ mice (Figures 3G and 3H). These data indicate that Nod1 normally localizes to DCGs in the presence of microbes or circulating microbial products.

Nod1 recruits Rab2a onto DCGs to regulate Chga retention in DCGs

We next sought to understand the molecular mechanism by which Nod1 affects the abundance of Chga in DCGs. Rabs, a family of small GTPases, are master regulators of intracellular membrane trafficking. Rab2a is known to be a Golgi-resident GTPase, governing intra-Golgi trafficking (Buffa et al., 2008; Ailion et al., 2014). In addition, Rab2a localizes to the membranes of lysosome-like organelles, such as DCGs, melanosomes and early endosomes. Studies have shown that Rab2a regulates cargo sorting events in neurons in *C. elegans* and intestinal Paneth cells (Edwards et al., 2009; Sumakovic et al., 2009; Zhang et al., 2015). In *C. elegans*, Rab2 null mutation impaired the maturation of the dense core of DCGs, and DCG cargos were mistargeted to early endosomes for degradation (Sumakovic et al., 2009; Edwards et al., 2009). In cultured intestinal organoids, Rab2a knockdown led to lysozyme being targeted for degradation in lysosomes instead of being stored in DCGs in Paneth cells (Zhang et al., 2015). Thus, we suspected that Rab2a might act downstream of Nod1 in regulating Chga storage in DCGs in chromaffin cells. We performed immunostaining of Rab2a and Nod1 in adrenal medulla (Figure S4A). We found that Rab2a and Nod1 largely colocalized in WT chromaffin cells (Figure S4A), consistent with our data showing that Nod1 localized to Rab10^{+} DCGs (Figure 3G). Consistently, our immunostaining showed Rab2a was recruited to synaptophysin^{+} DCGs in chromaffin cells in WT mice (Figure 4A). In comparison, the immunostaining signal of Rab2a on synaptophysin^{+} DCGs was greatly reduced in chromaffin cells from *Nod1*$^{-/-}$ mice (Figures 4A and S4B), whereas the protein level of Rab2a in isolated adrenal medullas from *Nod1*$^{-/-}$ mice was comparable with that from WT mice (Figure 4B), which indicates that the reduced immunostaining signal of Rab2a on DCGs in adrenal chromaffin cells from *Nod1*$^{-/-}$ mice was due to reduced recruitment. Furthermore, the immunostaining signal of Rab2a on synaptophysin^{+} DCGs was greatly reduced in chromaffin cells from ABX or *Lyz1*$^{-/-}$ mice (Figures 4C and S4C), whereas the protein level of Rab2a in isolated adrenal medullas from *Lyz1*$^{-/-}$ mice was comparable with that from WT mice (Figure 4B).

To determine whether Rab2a affects Chga retention in DCGs, we determined the effect of Rab2a on Chga in PC-12 cells. To perturb the activity of Rab2a, we created a Rab2a mutant, S20N, which was previously determined as a dominant negative mutant (Tisdale et al., 1992). By immunofluorescence staining, we compared the level of Chga between PC-12 cells transfected with eGFP empty vector (EV), designated eGFP(EV), eGFP-tagged Rab2a-WT, designated eGFP-Rab2a(WT), and cells transfected with eGFP-tagged Rab2a-S20N, designated eGFP-Rab2a(S20N) (Figure 4D). The expression of eGFP-Rab2a(S20N) led to a significant reduction in Chga protein level, indicated by reduced fluorescence intensity (Figures 4D–4F), compared to cells expressing eGFP(EV) or eGFP-tagged Rab2a-WT (Figures 4D–4F). It was previously shown that loss of Rab2a led to mistargeting of DCG cargos for degradation in lysosomes (Zhang et al., 2015; Edwards et al., 2009; Sumakovic et al., 2009). We treated PC-12 cells expressing Rab2a S20N with two different inhibitors of lysosome activity, leupeptin or chloroquine. Leupeptin or chloroquine treatment effectively restored Chga in cells expressing the Rab2a S20N mutant (Figures 4D–4F). Thus, Rab2a activity is involved in regulating the storage of Chga in DCGs.

Reduced catecholamine secretion in chromaffin cells deficient in Nod1 or Nod1 ligand

We next decided to address whether endogenous microbial Nod1 ligand might affect catecholamine secretion of chromaffin cells. We first employed the $GRAB_{NE}$ assay to compare the secretion activities of chromaffin cells isolated from WT, *Nod1*$^{-/-}$ and *Lyz1*$^{-/-}$ mice. Consistent with our result in Figure 1A, chromaffin cells from *Nod1*$^{-/-}$ mice displayed a defect in K^{+}-induced catecholamine secretion, compared to cells from WT mice (Figures 5A–5C). Deletion of Lyz1 also resulted in a marked defect in K^{+}-induced catecholamine secretion (Figures 5A–5C), albeit less severe than in cells from *Nod1*$^{-/-}$ mice. We wanted to determine whether supplementing Nod1 ligand could restore catecholamine secretion in *Lyz1*$^{-/-}$ mice. We orally supplemented *Lyz1*$^{-/-}$ mice with iE-DAP at a dose which restored the circulating level of Nod1 ligand *in vivo* in *Lyz1*$^{-/-}$ mice (Zhang et al., 2015). Orally supplementing *Lyz1*$^{-/-}$ mice with iE-DAP restored the secretion activity of *ex vivo* cultured chromaffin cells (Figures 5A–5C). This indicates that the lack of Nod1 ligand underlies the secretion defect in chromaffin cells in *Lyz1*$^{-/-}$ mice.

Next, we decided to determine the effect of Nod1 or its ligand on the dynamics of catecholamine secretion using single-cell amperometry. Single-cell amperometry measures the numbers of released catecholamine

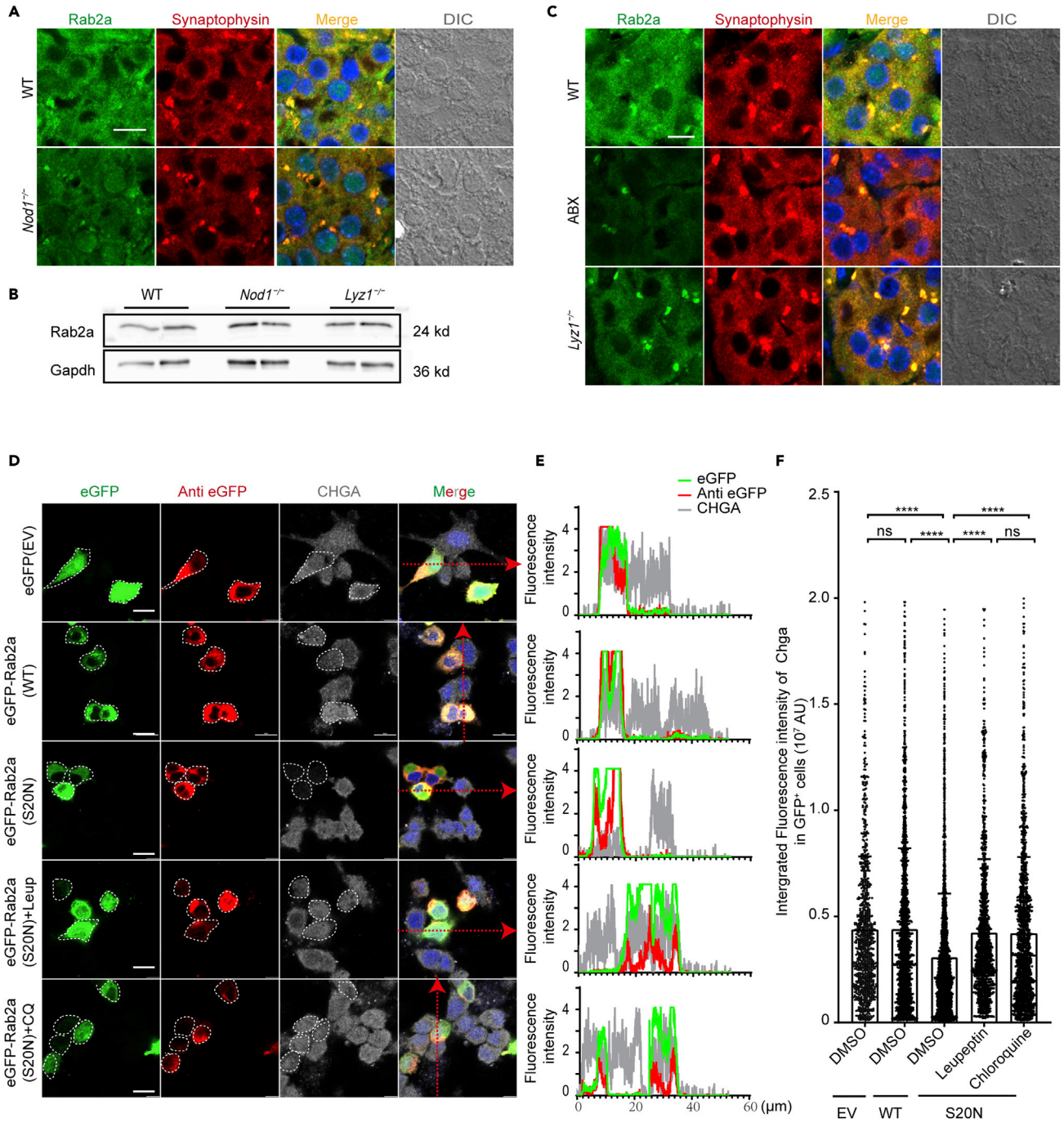

Figure 4. Nod1 recruits Rab2a onto DCGs to regulate Chga retention in DCGs

(A) Immunostaining and confocal imaging of Rab2a (green) and synaptophysin (red) in paraffin sections of adrenal glands from WT and *Nod1*$^{-/-}$ mice.

(B) Immunoblotting of Rab2a in isolated medullary regions from the indicated mice. Gapdh was used as a loading control.

(C) Immunostaining and confocal imaging of Rab2a (green) and synaptophysin (red) in paraffin sections of adrenal gland from WT, ABX, and *Lyz1*$^{-/-}$ mice.

(D) PC-12 cells were transfected with eGFP empty vector (EV), wild-type Rab2a tagged with eGFP, or a dominant-negative Rab2a-S20N mutant tagged with eGFP and then subjected to the indicated treatments. Cells were immunostained with anti-GFP (red) and anti-Chga (gray) antibodies. White dashed lines indicate the designated cell boundary.

(E) Fluorescence intensity analysis along the designated line on the left using Nikon-Elements Advanced Research Imaging Software.

(F) Fluorescence intensity of Chga staining in GFP-expressing cells shown in (D). At least 988 GFP^{+} cells (from more than 70 frames) were quantified per sample. Scale bars, 10 μm (A, C, and D). Each symbol represents one cell in (F). Statistically significant differences were determined using one-way ANOVA (F). ****$p < 0.0001$. ns, indicates no significant difference. Summary plot shows means and sd (F). Data (A-E) are representative of three independent experiments.

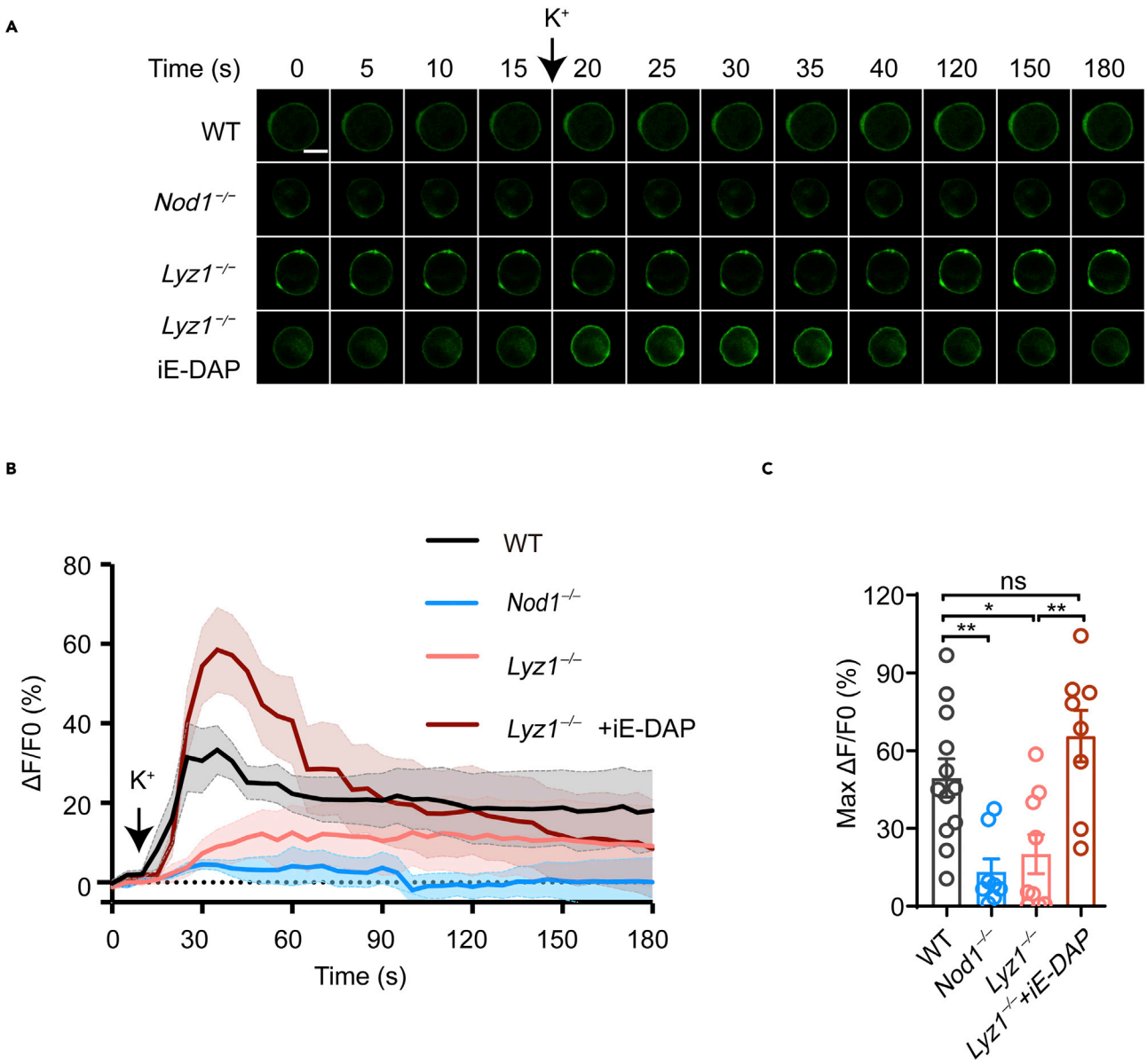

Figure 5. Endogenous Nod1 ligand modulates catecholamine secretion *ex vivo*

(A) Representative images of green fluorescence of $GRAB_{NE}$ in transfected chromaffin cells from WT, *Nod1*$^{-/-}$, *Lyz1*$^{-/-}$ mice, or *Lyz1*$^{-/-}$ mice orally gavaged with iE-DAP, during the course of treatment with K^+ solution (90 mM) to trigger secretion.

(B) The recorded relative fluorescence changes of $GRAB_{NE}$ over the time course of the experiment (ΔF/F0) (n = 8–12 cells from 5 to 8 mice).

(C) The maximum peak of ΔF/F0 in the different treatment groups from (B).

Scale bar, 5 μm (A). Each symbol represents a different cell (C). Statistically significant differences were determined using one-way ANOVA followed by Tukey's post hoc test (C). ns, not significant, *p < 0.05, **p < 0.01. Data are representative of three independent experiments.

molecules during every individual exocytosis event (Garcia et al., 2006; Wightman et al., 1991). Basically, catecholamines from each vesicle are captured and oxidized on a carbon electrode, resulting in a current (or amperometric) peak for each vesicle that bursts (Figure 6A). Each validated current peak represents a fusion event, and the number of catecholamine molecules from each fusion event is calculated from the integration of each single current event (Garcia et al., 2006; Wightman et al., 1991). Single-cell amperometry does not distinguish different kinds of catecholamines, but it can accurately quantify the number of molecules released and the kinetic parameters of each vesicle (Dunevall et al., 2015). Single-cell amperometry was employed to record each K^+-stimulated fusion event between secretory vesicles and the plasma

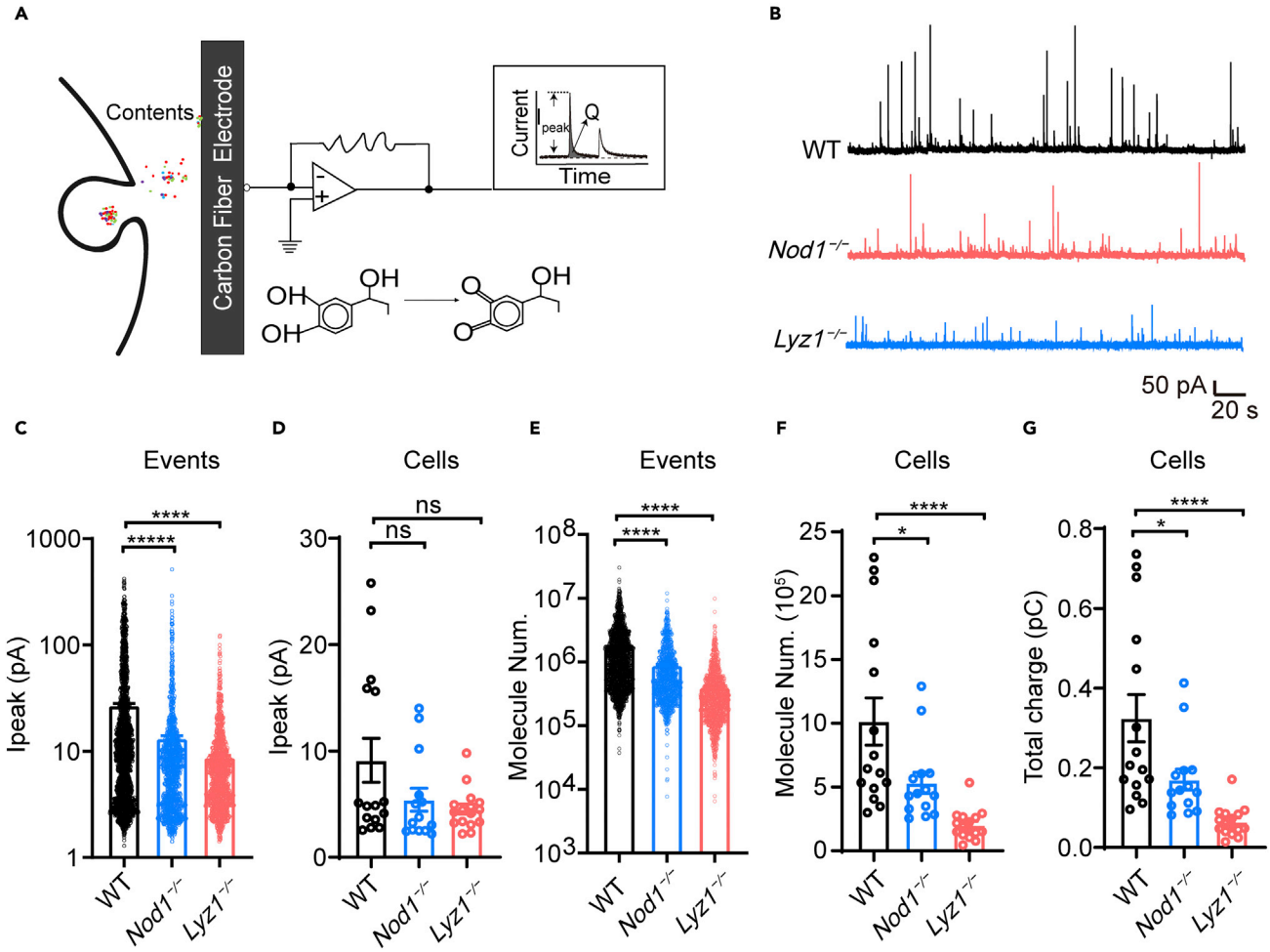

Figure 6. Amperometry recordings reveal a significant decrease in the number of catecholamine molecules released by individual vesicles in *Nod1*$^{-/-}$ and *Lyz1*$^{-/-}$ adrenal chromaffin cells

(A) Schematic diagram of the amperometry recording experiment.

(B) Representative amperometric traces from WT, *Nod1*$^{-/-}$, and Lyz1$^{-/-}$ chromaffin cells.

(C) Peak current of each amperometric spike event from WT (n = 2106 events), *Nod1*$^{-/-}$ (n = 1256 events), and *Lyz1*$^{-/-}$ (n = 1316 events) chromaffin cells.

(D) Medians of peak current from each WT (n = 15 cells), *Nod1*$^{-/-}$ (n = 14 cells), and *Lyz1*$^{-/-}$ (n = 16 cells) chromaffin cell were plotted with s.e.m.

(E) Number of molecules in each amperometric spike event from WT (n = 2106 events), *Nod1*$^{-/-}$ (n = 1256 events), and *Lyz1*$^{-/-}$ (n = 1316 events) chromaffin cells.

(F) Medians of number of molecules from each WT (n = 15 cells), *Nod1*$^{-/-}$ (n = 14 cells), and *Lyz1*$^{-/-}$ (n = 16 cells) chromaffin cells were plotted with s.e.m.

(G) Medians of total spike charge of each individual WT (n = 15 cells), *Nod1*$^{-/-}$ (n = 14 cells), and *Lyz1*$^{-/-}$ (n = 16 cells) chromaffin cell were plotted with s.e.m.

Statistically significant differences were determined using one-way ANOVA followed by Tukey's post hoc test (C-F). *p < 0.05, **p < 0.01, ****p < 0.001.

membrane on cultured primary chromaffin cells from WT, *Nod1*$^{-/-}$, and *Lyz1*$^{-/-}$ mice (Figure 6B). The distribution of the peak current of individual amperometric spike events was skewed toward lower values in *Nod1*$^{-/-}$ and *Lyz1*$^{-/-}$ chromaffin cells (Figure 6C). The means of peak current of individual event were significantly reduced in *Nod1*$^{-/-}$ and *Lyz1*$^{-/-}$ chromaffin cells compared with WT cells (Figure 6C), while the difference in medians of peak current of individual cells did not reach statistical significance (Figure 6D).

The numbers of catecholamine molecules released in each fusion event were calculated. The molecule numbers were significantly decreased per event in *Nod1*-or *Lyz1*-deficient cells (Figure 6E). This indicates that fewer catecholamine molecules were secreted per fusion event in *Nod1*$^{-/-}$ and *Lyz1*$^{-/-}$ chromaffin cells compared with WT cells. Comparing the medians of molecule numbers of individual cells also indicated a reduction in catecholamine secretion in *Nod1*$^{-/-}$ and *Lyz1*$^{-/-}$ chromaffin cells (Figure 6F).

Calculation of total spike charges also indicated less secretion of catecholamine in *Nod1*$^{-/-}$ and *Lyz1*$^{-/-}$ chromaffin cells (Figure 6G). Taken together, these data indicate that deficiency of Nod1 or Lyz1 leads to impaired catecholamine secretion from DCGs.

Deficiency of Nod1 ligand impairs the stress response

We wanted to determine the physiological function of Nod1 sensing in adrenal chromaffin cells. We employed a mouse immobilization model, which has been widely used to evaluate the adrenal medullary response during stress. The elevated epinephrine, together with other stress hormones, induces a range of physiological responses in preparation for the fight-or-flight response, including increased blood sugar level, glycogen mobilization in the liver, *etc* (Buira et al., 2004; Fernandez et al., 2000; Park et al., 2016; Kang et al., 2015). The plasma level of epinephrine reaches its peak from 30 min to 90 min after the onset of immobilization stress (Jeong et al., 2000; Kvetnansky et al., 2006; Qing et al., 2020). Thus, we subjected WT and *Lyz1*$^{-/-}$ mice to one hour of immobilization. WT and *Lyz1*$^{-/-}$ mice had comparable levels of circulating epinephrine under basal (non-stressed) conditions (Figure 7A). When the mice were immobilized for one hour, the level of circulating epinephrine markedly increased in WT mice, but the increase was blunted in *Lyz1*$^{-/-}$ mice (Figure 7A). We found that the blood sugar was clearly elevated in both *Lyz1*$^{-/-}$ and WT mice after restraint (Figure 7B), and the surge in blood sugar was less pronounced in *Lyz1*$^{-/-}$ mice (Figure 7B).

To further address more specifically whether Nod1 may affect epinephrine secretion in adrenal medulla, we depleted Nod1 in adrenal chromaffin cells by crossing *Dbh-cre* mice with *Nod1*$^{f/f}$ mice. The *Nod1* mRNA level was significantly reduced in the adrenomedullary region of *Dbh-cre;Nod1*$^{f/f}$ mice (Figure S5A). The staining signals of epinephrine and Chga were marked reduced in adrenal medullas in *Dbh-cre;Nod1*$^{f/f}$ mice compared with those in *Nod1*$^{f/f}$ mice (Figures S5B and S5C). Adrenal glands from *Dbh-cre;Nod1*$^{f/f}$ mice contained less epinephrine than control *Nod1*$^{f/f}$ mice, while the overall structure of adrenal gland and the relative ratio of medulla to whole adrenal gland were not changed in *Dbh-cre;Nod1*$^{f/f}$ mice (Figures S5D–S5J). We also performed the GRAB$_{NE}$ assay on cells isolated from *Dbh-cre;Nod1*$^{f/f}$ mice and control mice. K^+-stimulated epinephrine secretion was markedly blunted in cells from *Dbh-cre;Nod1*$^{f/f}$ mice compared with *Nod1*$^{f/f}$ or *Dbh-cre* controls (Figures S5K–S5M). To determine whether depletion of Nod1 in adrenal chromaffin cells might affect epinephrine *in vivo*, we subjected control and *Dbh-cre;Nod1*$^{f/f}$ mice to immobilization. Control and *Dbh-cre;Nod1*$^{f/f}$ mice had a comparable level of circulating epinephrine (Figure 7C). Immobilization resulted in a dramatic increase in the circulating epinephrine level in control mice, while the increase in epinephrine level was less pronounced in *Dbh-cre;Nod1*$^{f/f}$ mice (Figure 7C). The increase in blood sugar was also blunted in *Dbh-cre;Nod1*$^{f/f}$ mice compared with control mice (Figure 7D). Previous studies have shown that stress can result in significant depletion of liver glycogen within 20 or 30 min of the onset of immobilization (Sánchez et al., 2002; Fernández et al., 2000). We subjected mice to immobilization for 25 min. We found that the stress-induced depletion of the liver glycogen store in *Dbh-cre;Nod1*$^{f/f}$ mice was milder than in control mice (Figure 7E). Thus, our data demonstrate that Nod1 sensing in adrenal medulla is involved in epinephrine secretion during immobilization stress.

DISCUSSION

Here, we report that intestinal microbes modulate epinephrine output from adrenal medulla during immobilization stress. Mechanistically, we propose that upon sensing its ligand, Nod1 recruits Rab2a onto DCGs, which assists the retention of Chga and epinephrine in DCGs. Defects in this pathway lead to reduced epinephrine secretion. Thus, our study unveils a physiological role of Nod1-mediated cross talk between intestine and adrenal medulla to promote the epinephrine surge during the acute stress response.

Our *ex vivo* GRAB$_{NE}$ sensor assay revealed that exogenous iE-DAP enhanced epinephrine secretion in chromaffin cells in a Nod1-dependent manner, indicating a role of Nod1 in epinephrine secretion. It is notable that the *ex vivo* cultured *Nod1*$^{-/-}$ chromaffin cells had an impaired secretion response compared with WT chromaffin cells. It is possible that Nod1 plays ligand-dependent and ligand-independent roles in modulating epinephrine secretion. Epinephrine secretion from *ex vivo* cultured *Lyz1*$^{-/-}$ chromaffin cells was blunted, which indicates a ligand-dependent role of Nod1. However, it remains to be addressed whether Nod1 modulates epinephrine through ligand-independent manner. The PGN fragments sensed by adrenal glands are derived from intestinal microbes residing in the GI tract. To better mimic the route by which natural PGNs enter adrenal glands, we choose oral gavage to supplement the mice with iE-DAP.

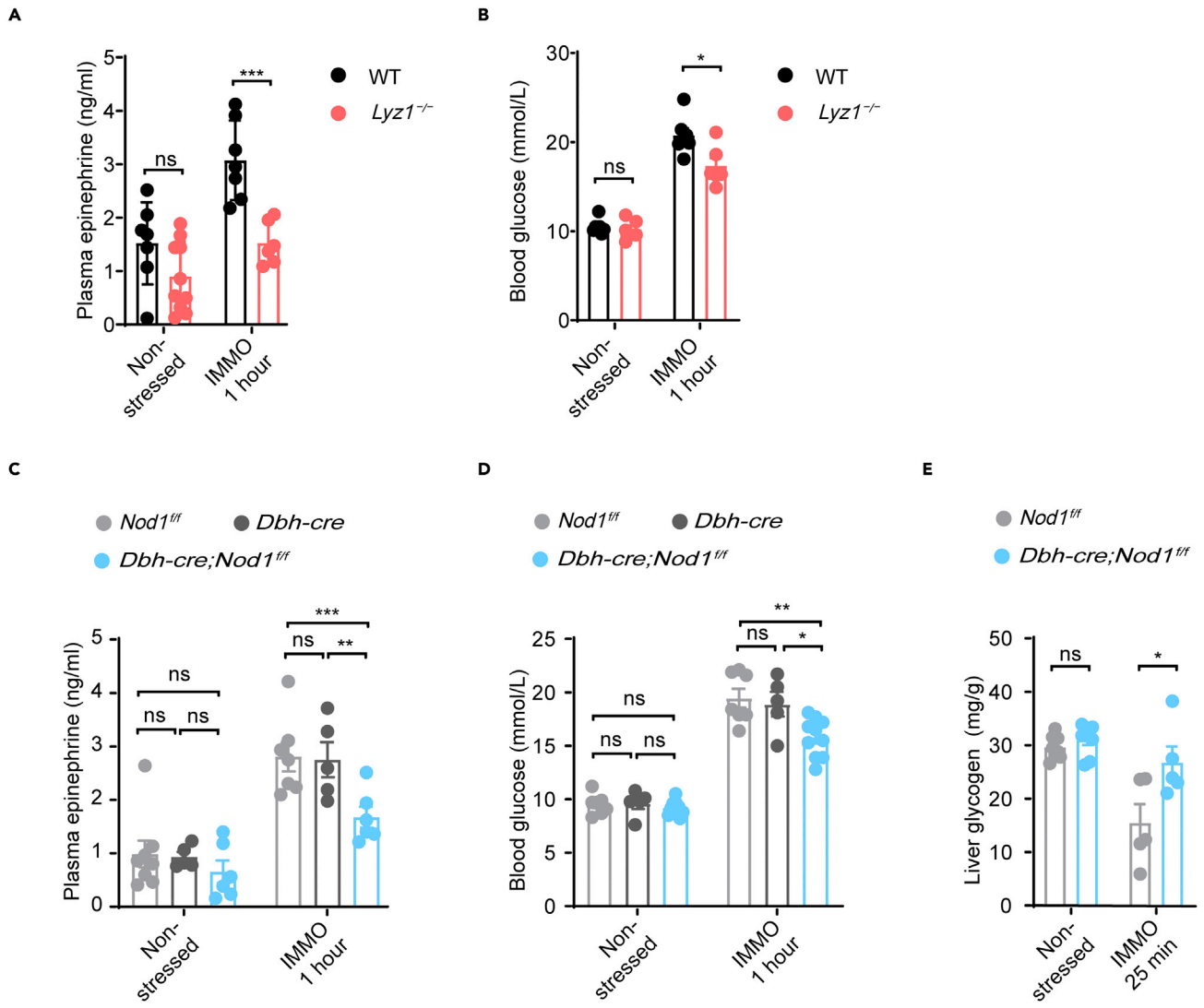

Figure 7. Deficiency of Nod1 ligand impairs epinephrine response

(A and C) Plasma level of epinephrine in the steady state and following stress induction by immobilization (IMMO; 1 hr) in WT (non-stressed, n = 7; IMMO 1 hr, n = 7), *Lyz1*$^{-/-}$ (non-stressed, n = 10; IMMO 1 hr, n = 6), *Dbh-cre* (non-stressed, n = 5; IMMO 1 hr, n = 5), *Nod1*$^{f/f}$ (non-stressed, n = 8; IMMO 1 hr, n = 7) and *Dbh-cre;Nod1*$^{f/f}$ (non-stressed, n = 6; IMMO 1 hr, n = 6) mice.

(B and D) Concentration of blood glucose in the steady state and following immobilization (IMMO; 1 hr) in WT (n = 7), *Lyz1*$^{-/-}$ (n = 6), *Dbh-cre* (n = 5), *Nod1*$^{f/f}$ (n = 7) and *Dbh-cre;Nod1*$^{f/f}$ (n = 10) mice.

(E) Liver glycogen content under steady-state conditions or after 25 min IMMO in *Nod1*$^{f/f}$ (non-stressed, n = 8; IMMO 1 hr, n = 5) and *Dbh-cre;Nod1*$^{f/f}$ (non-stressed, n = 8; IMMO 1 hr, n = 5) mice.

Statistically significant differences were determined using one-way ANOVA followed by Tukey's post hoc test (A-E). ns, indicates no significant difference ($p > 0.05$). *$p < 0.05$, **$p < 0.01$ and ***$p < 0.001$. Summary plots (A-E) show mean with s.e.m. Each symbol represents an individual mouse.

Oral supplementation of iE-DAP rescued the secretion defect of chromaffin cells from *Lyz1*$^{-/-}$ mice, indicating that optimal secretory activity of chromaffin cells from WT mice depends on the presence of endogenous Nod1 ligand. It is possible that endogenous Nod1 ligand remained bound in *ex vivo* cultured chromaffin cells from WT mice and regulated catecholamine secretion. It is also possible that the *ex vivo* cultured chromaffin cells from WT mice contained more epinephrine when initially isolated, and more epinephrine was secreted upon stimulation during the $GRAB_{NE}$ assay.

Nod1 expression is known in immune-related tissues, such as spleen and lung. In this study, we found that the adrenal medullary region expressed a high level of Nod1. Notably, the expression of Nod1 in adrenal

gland was restricted to the medulla region, as evidenced by our immunohistochemistry and quantitative PCR results. In comparison, the overall level of *Nod1* mRNA in adrenal gland remained relatively low, consistent with online databases. Interestingly, our previous study found a highly restricted expression of Nod1 in pancreatic beta cells but not in other pancreatic cells (Zhang et al., 2015). RNA-seq data showed selectively higher expression of Nod1 in adrenal chromaffin cells compared to sympathetic nerves (Chan et al., 2019). Thus, we suspect that Nod1, despite not being widely expressed, is selectively expressed in small subsets of cells in certain tissues, which might be involved in responding to bacterial PGNs.

Adrenal chromaffin cells are the primary source of epinephrine during the immobilization-induced stress response. We employed the immobilization method to evaluate the role of Nod1 in epinephrine secretion. A mouse *Dbh-cre* line was used to deplete Nod1. In addition to adrenal chromaffin cells, Dbh is also expressed in certain neurons and sympathetic nerves. Thus, we cannot exclude the possibility that Nod1 may play roles in catecholaminergic Dbh^{+} cells other than adrenal chromaffin cells during the stress response. However, our analysis on ex *vivo* cultured primary chromaffin cells supports a cell-intrinsic role of Nod1. It remains to be determined whether Nod1 expressed in cells other than intestinal epithelium and adrenal chromaffin cells may regulate other aspects of physiological processes involved in the stress response.

Studies have revealed that GF and ABX mice displayed reduced anxiety-like behavior compared with SPF controls. Previous studies had demonstrated that the HPA axis and serotonergic system were altered in mice lacking microbiota (Sudo et al., 2004; Clarke et al., 2013; Zheng et al., 2016). The adrenomedullary response, HPA axis and hippocampal serotonergic system are tightly integrated in regulating stress, anxiety and depression. Our study indicates a role of Nod1 in regulating the adrenomedullary response by regulating epinephrine storage and secretion. It is worth noting that 5-HT can exert an inhibitory effect on epinephrine secretion from adrenal chromaffin cells (Brindley et al., 2016). It has been shown that adrenal chromaffin cells recycle 5-HT through serotonin transporter (SERT) (Brindley et al., 2016; Linder et al., 2009). Deficiency of SERT resulted in reduction of 5-HT in adrenal gland and enhanced secretion of epinephrine without affecting the adrenal gland epinephrine content. In primary cultured chromaffin cells, 5-HT treatment reduced the number of vesicles undergoing exocytosis, without affecting the quantal size and kinetics of transmitter release from individual vesicular fusion events (Brindley et al., 2016, 2017). Previously, Nod1 has been implicated in the 5-HT signaling pathway. Mice deficient in both Nod1 and Nod2 exhibited signs of stress-induced anxiety-like behavior and had lower levels of 5-HT in both the hippocampus and brainstem, through a mechanism that partially depended on Nod1 expressed in the intestinal epithelium (Pusceddu et al., 2019). Indeed, another study found that Nod1 activation reduced the SERT mRNA level in an intestinal epithelial cell line (Layunta et al., 2018). However, our quantitative PCR showed that depletion of Nod1 did not affect the SERT mRNA level in adrenal chromaffin cells. Furthermore, our single-cell amperometry showed reduced quantal size and kinetics of individual vesicular fusion events in chromaffin cells from $Nod1^{-/-}$ and $Lyz1^{-/-}$ mice, indicating a mechanism distinct from 5-HT recycling. Therefore, the effect of microbial Nod1 ligand on epinephrine storage and secretion is independent of 5-HT signaling.

We found that loss of Nod1 or microbial Nod1 ligand results in impaired storage and secretion of epinephrine in DCGs. $Nod1^{-/-}$ and $Lyz1^{-/-}$ mice had lower levels of Chga and epinephrine. Chga has been shown to regulate the biogenesis of catecholamine-containing DCGs in the adrenal gland (Díaz-Vera et al., 2012; Kim et al., 2001; Pasqua et al., 2016). We attribute the reduced storage of epinephrine to the reduced amount of Chga. Previous work found that the absence of gut microbial colonization selectively impaired the catecholamine response to hypoglycemic stress in mice, and the transcriptome in adrenal glands was altered (Giri et al., 2019). However, the amounts of epinephrine and Chga in adrenal glands were not analyzed. It remains to be determined whether Nod1-regulated storage of epinephrine may also contribute to the impaired catecholamine response to hypoglycemic stress.

Previous findings have found that Nod1 and Nod2 undergo enhanced membrane recruitment upon ligand binding (Lu et al., 2019). Indeed, our previous studies have shown enhanced membrane recruitment of Nod1 and Nod2 upon commensal bacterial colonization in β cells and intestinal Paneth cells, respectively (Zhang et al., 2019). In this study, immunostaining showed Nod1 largely localized to DCGs in chromaffin

cells in WT mice, and ABX treatment or Lyz1 depletion greatly reduced the staining signal of Nod1 on DCGs. Meanwhile, our immunoblotting and quantitative PCR showed comparable levels of Nod1 protein and mRNA present in medullas in WT and *Lyz1*$^{-/-}$ mice. Thus, we attributed the reduced staining of Nod1 on DCGs to the reduced membrane recruitment of Nod1 onto DCGs. Our immunostaining procedure on paraffin-embedded tissues might have favored the visualization of membrane-localized proteins, which we have previously encountered (Zhang et al., 2015, 2019). We suspect that the amount of cytosolic Nod1 was underestimated in our staining. Nevertheless, our data support that the recruitment of Nod1 onto DCGs can be enhanced by microbial Nod1 ligand.

Our electron microscopy (EM) analysis revealed enlarged DCGs and less condensed DCG cores in chromaffin cells in in *Nod1*$^{-/-}$ mice, a defect similar to that reported for Chga KO mice in the C57BL/6J background (Pasqua et al., 2016). We found that *Chga* mRNA levels were not affected in adrenal medullas of *Nod1*$^{-/-}$ mice, while Chga protein levels were reduced by half. We observed reduced recruitment of Rab2a onto DCGs in *Nod1*$^{-/-}$, *Lyz1*$^{-/-}$, and ABX mice. Overexpressing a dominant negative mutant of Rab2a reduced the level of Chga in PC-12 cells, and this phenotype was reversed by inhibiting the activity of lysosomes. We propose a scenario where a reduced level of Nod1 or Nod1 ligand impairs Rab2a recruitment onto DCG membranes, which may cause mistargeting of a significant proportion of Chga to lysosomes for degradation. The involvement of Rab2a in DCG cargo sorting has been previously reported (Edwards et al., 2009; Sugawara et al., 2014; Sumakovic et al., 2009; Zhang et al., 2015). Loss of Rab2a in neurons in *C. elegans* led to specific lysosomal degradation of a neuropeptide that is normally located in DCGs (Edwards et al., 2009; Sumakovic et al., 2009). Knockdown of Rab2a led to lysosomal degradation of lysozyme in intestinal Paneth cells (Zhang et al., 2015). Besides DCGs, Rab2a also functions at various steps of intracellular membrane trafficking, including endoplasmic reticulum (ER)-Golgi transport, autophagy and autolysosome formation, and endosome-lysosome fusion. Indeed, our results showed that Nod1 localized to a region close to nuclei, together with Rab2a, in chromaffin cells from ABX or *Lyz1*$^{-/-}$ mice. Therefore, Nod1 together with Nod1 ligand is required to recruit Rab2a onto DCGs. We suspect some other factors downstream of Nod1 are involved in recruiting Rab2a onto DCGs, which warrants further investigation.

Although Nod1 is well recognized as a peptidoglycan receptor involved in inflammation, investigations into the mechanisms that mediate cross talk between host and commensal microbes have uncovered a much more complex role of Nod1. For instance, Nod1, activated by the Nod1 ligand, instructs the maturation of gut-associated lymphoid tissues in mice (Bouskra et al., 2008). Nod1 signaling primes neutrophils for optimal bactericidal activity (Clarke et al., 2010). Nod1 signaling in mesenchymal stromal cells regulates hematopoiesis (Iwamura et al., 2017). Nod1 signaling contributes to metabolic inflammation during high fat diet-induced obesity (Schertzer et al., 2011). Beyond immunity and inflammation, Nod1 sensing regulates 5-HT signaling in intestinal epithelium and regulates insulin trafficking in islet beta cells (Pusceddu et al., 2019; Zhang et al., 2019). Despite extensive evidence that Nod1 mediates the cross talk between host and commensal bacteria, it remains largely unanswered how Nod1 ligand derived from commensal bacteria gets into various host cells. It was previously reported that oligopeptide transporters encoded by SLC15A3 and SLC15A4 are responsible for transporting small PGN fragments into macrophages (Nakamura et al., 2014). Whether such transporters mediate import of Nod1 ligand from the circulation into Nod1-expressing cells remains to be determined.

In summary, Nod1 ligand from intestinal microbes directly modulates the storage of Chga and epinephrine in DCGs in adrenal chromaffin cells, which optimizes epinephrine secretion under stress conditions. Thus, our study further exemplifies Nod1 ligand as a key signaling molecule in the microbiota-intestine-brain axis.

Limitations of the study

In this study, we demonstrated that adrenal chromaffin cells respond to colonization of commensal bacterial through sensing soluble molecule, such as Nod1 ligand, from commensal bacteria. Our *ex vivo* experiments show an effect of Nod1 ligand on isolated adrenal chromaffin cells. Although the *ex vivo* system offers an opportunity to dissect the molecular mechanisms, the interactions between bacteria and SAM *in vivo* are likely more complicated. We used *Lyz1*$^{-/-}$ mice or *Dbh-cre;Nod1*$^{f/f}$ mice for our *in vivo* experiments to demonstrate the effect of bacterial Nod1. However, both animal models have their drawbacks. Other bacterial ligands could be altered in *Lyz1*$^{-/-}$ mice, while cells other than chromaffin cells could be

affected in *Dbh-cre;Nod1*$^{f/f}$ mice. The effects of bacterial colonization on the stress response are likely coordinated by an array of different bacterial components and a number of host cells and sensors. The effect of bacterial Nod1 ligand on epinephrine secretion reflects one aspect of bacteria-host cross talk during stress response. The modulatory roles of commensal bacteria on stress response warrant further investigation and will be an exciting area for future research.

STAR★METHODS

Detailed methods are provided in the online version of this paper and include the following:

- KEY RESOURCES TABLE
- RESOURCE AVAILABILITY
  - Lead contact
  - Materials availability
  - Data and code availability
- EXPERIMENTAL MODEL AND SUBJECT DETAILS
  - Mice
- METHOD DETAILS
  - Plasmids
  - ABX treatments
  - Oral iE-DAP supplementation to mice
  - PC-12 cell culture, transfection, immunofluorescence staining and image quantification
  - Adrenal gland dissection and size analysis
  - Isolation and culture of mouse adrenal chromaffin cells
  - Amperometric recording and analysis
  - Characterization of $GRAB_{NE}$ in PC-12 cells
  - *Ex vivo* K^+-stimulated catecholamine secretion assay ($GRAB_{NE}$ assay)
  - Extraction of adrenal glands
  - Immobilization and plasma preparation
  - Epinephrine quantification
  - Detection of glycogen
  - Immunofluorescence (IF) staining and immunohistochemistry staining of tissue sections
  - Image analysis and quantification
  - Gene expression analysis using quantitative reverse-transcription PCR
  - Western blotting
  - Electron microscopic analysis of DCGs in adrenal chromaffin cells
- QUANTIFICATION AND STATISTICAL ANALYSIS

SUPPLEMENTAL INFORMATION

Supplemental information can be found online at https://doi.org/10.1016/j.isci.2021.102849.

ACKNOWLEDGMENTS

We thank Jiesi Feng and Yulong Li (State Key Laboratory of Membrane Biology, Peking University School of Life Sciences, Beijing) for the pDisplay-NE1m-IRES-mCherry-CAAX plasmid; Cheng Zhan (National Institute of Biological Sciences, Beijing, China) for the *Dbh-Cre* mouse strain; and Yihui Xu and the service station of CAS key laboratory of infection and immunity for technical support. This work was supported by the National Key Research and Development Program of China (Grant no. 2017YFA0503403 and 2018YFE0207300), the National Natural Science Foundation of China (Grant no. 31730028 and 81670482), the Instrument Development Project, CAS (YJKYYQ20180028 to J.S.), the National Natural Science Foundation of China (31527802 to J.S.), CAS Key Laboratory of Brain Connectome and Manipulation, NO. 2019DP173024, and Youth Innovation Promotion Association of the Chinese Academy of Sciences of China NO. 2017130 (P.C.).

AUTHOR CONTRIBUTIONS

Conceptualization, J.S. and Z.L.; methodology, C.X., P.C., and Z.L.; investigation, C.X., P.C., Z.L., Q.Z., Y.P., Y.L., and W.X.; writing – original draft, C.X., P.C., and Z.L.; writing–review & editing, C.X. and Z.L.; funding acquisition, P.C., J.S., and Z.L.; supervision, Z.L. and J.S.

DECLARATION OF INTERESTS

No competing interests declared.

Received: February 22, 2021
Revised: June 7, 2021
Accepted: July 9, 2021
Published: August 20, 2021

REFERENCES

Ailion, M., Hannemann, M., Dalton, S., Pappas, A., Watanabe, S., Hegermann, J., Liu, Q., Han, H.F., Gu, M., Goulding, M.Q., et al. (2014). Two Rab2 interactors regulate dense-core vesicle maturation. Neuron *82*, 167–180.

Arentsen, T., Qian, Y., Gkotzis, S., Femenia, T., Wang, T., Udekwu, K., Forssberg, H., and Diaz Heijtz, R. (2017). The bacterial peptidoglycan-sensing molecule Pglyrp2 modulates brain development and behavior. Mol. Psychiatry *22*, 257–266.

Bird, L. (2010). A NOD to neutrophils. Nat. Rev. Immunol. *10*, 157.

Blander, J.M., Longman, R.S., Iliev, I.D., Sonnenberg, G.F., and Artis, D. (2017). Regulation of inflammation by microbiota interactions with the host. Nat. Immunol. *18*, 851–860.

Bouskra, D., Brezillon, C., Berard, M., Werts, C., Varona, R., Boneca, I.G., and Eberl, G. (2008). Lymphoid tissue genesis induced by commensals through NOD1 regulates intestinal homeostasis. Nature *456*, 507–510.

Brindley, R.L., Bauer, M.B., Blakely, R.D., and Currie, K.P.M. (2016). An interplay between the serotonin transporter (SERT) and 5-HT receptors controls stimulus-secretion coupling in sympathoadrenal chromaffin cells. Neuropharmacology *110*, 438–448.

Brindley, R.L., Bauer, M.B., Blakely, R.D., and Currie, K.P.M. (2017). Serotonin and serotonin transporters in the adrenal medulla: a potential hub for modulation of the sympathetic stress response. ACS Chem. Neurosci. *8*, 943–954.

Buffa, L., Fuchs, E., Pietropaolo, M., Barr, F., and Solimena, M. (2008). ICA69 is a novel Rab2 effector regulating ER-Golgi trafficking in insulinoma cells. Eur. J. Cell Biol. *87*, 197–209.

Buira, I., Poch, E., Sanchez, O., Fernandez-Varo, G., Grau, M., Tebar, F., Ramirez, I., and Soley, M. (2004). Sialoadenectomy alters liver cell turn-over and function in mice. J. Cell. Physiol. *198*, 12–21.

Chan, K.L., Tam, T.H., Boroumand, P., Prescott, D., Costford, S.R., Escalante, N.K., Fine, N., Tu, Y., Robertson, S.J., Prabaharan, D., et al. (2017). Circulating NOD1 activators and hematopoietic NOD1 contribute to metabolic inflammation and insulin resistance. Cell Rep. *18*, 2415–2426.

Chan, W.H., Komada, M., Fukushima, T., Southard-Smith, E.M., Anderson, C.R., and Wakefield, M.J. (2019). RNA-seq of isolated chromaffin cells highlights the role of sex-linked and imprinted genes in adrenal medulla development. Sci. Rep. *9*, 3929.

Chen, P., Shen, X., Zhao, S., Liu, Z., Zhu, Q., Zhu, T., Zhang, S., Li, Y., Mao, L., and Sun, J. (2021). Measurement of intact quantal packet of transmitters released from single nerve terminal by loose-patch amperometry. Biosens. Bioelectron. *181*, 113143.

Clarke, G., Grenham, S., Scully, P., Fitzgerald, P., Moloney, R.D., Shanahan, F., Dinan, T.G., and Cryan, J.F. (2013). The microbiome-gut-brain axis during early life regulates the hippocampal serotonergic system in a sex-dependent manner. Mol. Psychiatry *18*, 666–673.

Clarke, T.B., Davis, K.M., Lysenko, E.S., Zhou, A.Y., Yu, Y., and Weiser, J.N. (2010). Recognition of peptidoglycan from the microbiota by Nod1 enhances systemic innate immunity. Nat. Med. *16*, 228–231.

Crumeyrolle-Arias, M., Jaglin, M., Bruneau, A., Vancassel, S., Cardona, A., Dauge, V., Naudon, L., and Rabot, S. (2014). Absence of the gut microbiota enhances anxiety-like behavior and neuroendocrine response to acute stress in rats. Psychoneuroendocrinology *42*, 207–217.

Díaz-Vera, J., Camacho, M., Machado, J.D., Domínguez, N., Montesinos, M.S., Hernández-Fernaud, J.R., Luján, R., and Borges, R. (2012). Chromogranins A and B are key proteins in amine accumulation, but the catecholamine secretory pathway is conserved without them. FASEB J. *26*, 430–438.

Diaz Heijtz, R., Wang, S., Anuar, F., Qian, Y., Bjorkholm, B., Samuelsson, A., Hibberd, M.L., Forssberg, H., and Pettersson, S. (2011). Normal gut microbiota modulates brain development and behavior. Proc. Natl. Acad. Sci. U S A *108*, 3047–3052.

Dunevall, J., Fathali, H., Najafinobar, N., Lovric, J., Wigstrom, J., Cans, A.S., and Ewing, A.G. (2015). Characterizing the catecholamine content of single mammalian vesicles by collision-adsorption events at an electrode. J. Am. Chem. Soc. *137*, 4344–4346.

Edwards, S.L., Charlie, N.K., Richmond, J.E., Hegermann, J., Eimer, S., and Miller, K.G. (2009). Impaired dense core vesicle maturation inCaenorhabditis elegansmutants lacking Rab2. J. Cell Biol. *186*, 881–895.

Farzi, A., Frohlich, E.E., and Holzer, P. (2018). Gut microbiota and the neuroendocrine system. Neurotherapeutics *15*, 5–22.

Farzi, A., Reichmann, F., Meinitzer, A., Mayerhofer, R., Jain, P., Hassan, A.M., Frohlich, E.E., Wagner, K., Painsipp, E., Rinner, B., and Holzer, P. (2015). Synergistic effects of NOD1 or NOD2 and TLR4 activation on mouse sickness behavior in relation to immune and brain activity markers. Brain Behav. Immun. *44*, 106–120.

Feng, J., Zhang, C., Lischinsky, J.E., Jing, M., Zhou, J., Wang, H., Zhang, Y., Dong, A., Wu, Z., Wu, H., et al. (2019). A genetically encoded fluorescent sensor for rapid and specific in vivo detection of norepinephrine. Neuron *102*, 745–761.e8.

Fenwick, E.M., Marty, A., and Neher, E. (1982). A patch-clamp study of bovine chromaffin cells and of their sensitivity to acetylcholine. J. Physiol. *331*, 577–597.

Fernández, G., Mena, M.-P., Arnau, A., Sánchez, O., Soley, M., and Ramírez, I. (2000). Immobilization stress induces c-Fos accumulation in liver. Cell Stress Chaperones *5*, 306.

Fernandez, G., Mena, M.P., Arnau, A., Sanchez, O., Soley, M., and Ramirez, I. (2000). Immobilization stress induces c-Fos accumulation in liver. Cell Stress Chaperones *5*, 306–312.

Foster, J.A., and McVey Neufeld, K.A. (2013). Gut-brain axis: how the microbiome influences anxiety and depression. Trends Neurosci. *36*, 305–312.

Fung, T.C., Olson, C.A., and Hsiao, E.Y. (2017). Interactions between the microbiota, immune and nervous systems in health and disease. Nat. Neurosci. *20*, 145–155.

Garcia, A.G., Garcia-De-Diego, A.M., Gandia, L., Borges, R., and Garcia-Sancho, J. (2006). Calcium signaling and exocytosis in adrenal chromaffin cells. Physiol. Rev. *86*, 1093–1131.

Gerfen, C.R., Paletzki, R., and Heintz, N. (2013). GENSAT BAC cre-recombinase driver lines to study the functional organization of cerebral cortical and basal ganglia circuits. Neuron *80*, 1368–1383.

Giri, P., Hu, F., La Gamma, E.F., and Nankova, B.B. (2019). Absence of gut microbial colonization attenuates the sympathoadrenal response to hypoglycemic stress in mice: implications for human neonates. Pediatr. Res. *85*, 574–581.

Greene, L.A., and Tischler, A.S. (1976). Establishment of a noradrenergic clonal line of rat adrenal pheochromocytoma cells which respond to nerve growth-factor. Proc. Natl. Acad. Sci. U S A *73*, 2424–2428.

Hergott, C.B., Roche, A.M., Tamashiro, E., Clarke, T.B., Bailey, A.G., Laughlin, A., Bushman, F.D.,

and Weiser, J.N. (2016). Peptidoglycan from the gut microbiota governs the lifespan of circulating phagocytes at homeostasis. Blood *127*, 2460–2471.

Hill, D.A., Hoffmann, C., Abt, M.C., Du, Y., Kobuley, D., Kirn, T.J., Bushman, F.D., and Artis, D. (2010). Metagenomic analyses reveal antibiotic-induced temporal and spatial changes in intestinal microbiota with associated alterations in immune cell homeostasis. Mucosal Immunol. *3*, 148–158.

Huo, R., Zeng, B., Zeng, L., Cheng, K., Li, B., Luo, Y., Wang, H., Zhou, C., Fang, L., Li, W., et al. (2017). Microbiota modulate anxiety-like behavior and endocrine abnormalities in hypothalamic-pituitary-adrenal Axis. Front. Cell. Infect. Microbiol. *7*, 489.

Inohara, N., Koseki, T., Del Peso, L., Hu, Y., Yee, C., Chen, S., Carrio, R., Merino, J., Liu, D., Ni, J., and Nunez, G. (1999). Nod1, an Apaf-1-like activator of caspase-9 and nuclear factor-kappaB. J. Biol. Chem. *274*, 14560–14567.

Iwamura, C., Bouladoux, N., Belkaid, Y., Sher, A., and Jankovic, D. (2017). Sensing of the microbiota by NOD1 in mesenchymal stromal cells regulates murine hematopoiesis. Blood *129*, 171–176.

Jeong, K.-H., Jacobson, L., Pacak, K., Widmaier, E.P., Goldstein, D.S., and Majzoub, J.A. (2000). Impaired basal and restraint-induced epinephrine secretion in corticotropin-releasing hormone- deficient mice*. Endocrinology *141*, 1142–1150.

Kang, Y.J., Sim, Y.B., Park, S.H., Sharma, N., and Suh, H.W. (2015). Involvement of alpha(2)-adrenergic receptor in the regulation of the blood glucose level induced by immobilization stress. Arch. Pharm. Res. *38*, 921–929.

Kim, T., Tao-Cheng, J.H., Eiden, L.E., and Loh, Y.P. (2001). Chromogranin A, an "on/off" switch controlling dense-core secretory granule biogenesis. Cell *106*, 499–509.

Kolski-Andreaco, A., Cai, H., Currle, D.S., Chandy, K.G., and Chow, R.H. (2007). Mouse adrenal chromaffin cell isolation. J. Vis. Exp. *2*, 129.

Kvetnansky, R., Kubovcakova, L., Tillinger, A., Micutkova, L., Krizanova, O., and Sabban, E. (2006). Gene expression of phenylethanolamine N-methyltransferase in corticotropin-releasing hormone knockout mice during stress exposure. Cell Mol. Neurobiol. *26*, 733–752.

Layunta, E., Latorre, E., Forcen, R., Grasa, L., Plaza, M.A., Arias, M., Alcalde, A.I., and Mesonero, J.E. (2018). NOD1 downregulates intestinal serotonin transporter and interacts with other pattern recognition receptors. J. Cell. Physiol. *233*, 4183–4193.

Linder, A.E., Beggs, K.M., Burnett, R.J., and Watts, S.W. (2009). Body distribution of infused serotonin in rats. Clin. Exp. Pharmacol. Physiol. *36*, 599–601.

Liu, J., Buisman-Pijlman, F., and Hutchinson, M.R. (2014). Toll-like receptor 4: innate immune regulator of neuroimmune and neuroendocrine interactions in stress and major depressive disorder. Front. Neurosci. *8*, 309.

Lu, Y., Zheng, Y.P., Coyaud, E., Zhang, C., Selvabaskaran, A., Yu, Y.Y., Xu, Z.Z., Weng, X.L., Chen, J.S., Meng, Y., et al. (2019). Palmitoylation of NOD1 and NOD2 is required for bacterial sensing. Science *366*, 460.

Luo, Y., Zeng, B., Zeng, L., Du, X., Li, B., Huo, R., Liu, L., Wang, H., Dong, M., Pan, J., et al. (2018). Gut microbiota regulates mouse behaviors through glucocorticoid receptor pathway genes in the hippocampus. Transl. Psychiatry *8*, 187.

Meunier, F.A., Álvarez, Y.D., Belingheri, A.V., Perez Bay, A.E., Javis, S.E., Tedford, H.W., Zamponi, G., and Marengo, F.D. (2013). The immediately releasable pool of mouse chromaffin cell vesicles is coupled to P/Q-Type calcium channels via the synaptic protein interaction site. PLoS One *8*, e54846.

Mosharov, E.V., and Sulzer, D. (2005). Analysis of exocytotic events recorded by amperometry. Nat. Methods *2*, 651–658.

Muller, A., Joseph, V., Slesinger, P.A., and Kleinfeld, D. (2014). Cell-based reporters reveal in vivo dynamics of dopamine and norepinephrine release in murine cortex. Nat. Methods *11*, 1245–1252.

Nakamura, N., Lill, J.R., Phung, Q., Jiang, Z., Bakalarski, C., De Maziere, A., Klumperman, J., Schlatter, M., Delamarre, L., and Mellman, I. (2014). Endosomes are specialized platforms for bacterial sensing and NOD2 signalling. Nature *509*, 240–244.

Nicholson, J.K., Holmes, E., Kinross, J., Burcelin, R., Gibson, G., Jia, W., and Pettersson, S. (2012). Host-gut microbiota metabolic interactions. Science *336*, 1262–1267.

Park, S.-H., Sim, Y.-B., Kim, S.-S., Lee, J.-R., Sharma, N., and Suh, H.-W. (2016). Effects of 5,7-dihroxytryptamine administered supraspinally or spinally on the blood glucose level in D-glucose-fed and immobilization stress models. Anim. Cells Syst. *20*, 289–295.

Pasqua, T., Mahata, S., Bandyopadhyay, G.K., Biswas, A., Perkins, G.A., Sinha-Hikim, A.P., Goldstein, D.S., Eiden, L.E., and Mahata, S.K. (2016). Impact of chromogranin a deficiency on catecholamine storage, catecholamine granule morphology and chromaffin cell energy metabolism in vivo. Cell Tissue Res. *363*, 693–712.

Pusceddu, M.M., Barboza, M., Keogh, C.E., Schneider, M., Stokes, P., Sladek, J.A., Kim, H.J.D., Torres-Fuentes, C., Goldfild, L.R., Gillis, S.E., et al. (2019). Nod-like receptors are critical for gut-brain axis signalling in mice. J. Physiol. *597*, 5777–5797.

Qing, H., Desrouleaux, R., Israni-Winger, K., Mineur, Y.S., Fogelman, N., Zhang, C., Rashed, S., Palm, N.W., Sinha, R., and Picciotto, M.R. (2020). Origin and function of stress-induced IL-6 in murine models. Cell *182*, 372–387. e14.

Rogers, G.B., Keating, D.J., Young, R.L., Wong, M.L., Licinio, J., and Wesselingh, S. (2016). From gut dysbiosis to altered brain function and mental illness: mechanisms and pathways. Mol. Psychiatry *21*, 738–748.

Rooks, M.G., and Garrett, W.S. (2016). Gut microbiota, metabolites and host immunity. Nat. Rev. Immunol. *16*, 341–352.

Sala, F., Nistri, A., and Criado, M. (2008). Nicotinic acetylcholine receptors of adrenal chromaffin cells. Acta Physiol. *192*, 203–212.

Sánchez, O., Arnau, A., Pareja, M., Poch, E., Ramírez, I., and Soley, M. (2002). Acute stress-induced tissue injury in mice: differences between emotional and social stress. Cell Stress Chaperones *7*, 36.

Schertzer, J.D., Tamrakar, A.K., Magalhaes, J.G., Pereira, S., Bilan, P.J., Fullerton, M.D., Liu, Z., Steinberg, G.R., Giacca, A., Philpott, D.J., and Klip, A. (2011). NOD1 activators link innate immunity to insulin resistance. Diabetes *60*, 2206–2215.

Shanks, N., Larocque, S., and Meaney, M.J. (1995). Neonatal endotoxin exposure alters the development of the hypothalamic-pituitary-adrenal Axis - early illness and later responsivity to stress. J. Neurosci. *15*, 376–384.

Shihan, M.H., Novo, S.G., Le Marchand, S.J., Wang, Y., and Duncan, M.K. (2021). A simple method for quantitating confocal fluorescent images. Biochem. Biophys. Rep. *25*, 100916.

Stojanovic, O., and Trajkovski, M. (2019). Microbiota guides insulin trafficking in beta cells. Cell Res. *29*, 603–604.

Sudo, N., Chida, Y., Aiba, Y., Sonoda, J., Oyama, N., Yu, X.N., Kubo, C., and Koga, Y. (2004). Postnatal microbial colonization programs the hypothalamic-pituitary-adrenal system for stress response in mice. J. Physiol. *558*, 263–275.

Sugawara, T., Kano, F., and Murata, M. (2014). Rab2A is a pivotal switch protein that promotes either secretion or ER-associated degradation of (pro)insulin in insulin-secreting cells. Sci. Rep. *4*, 6952.

Sumakovic, M., Hegermann, J., Luo, L., Husson, S.J., Schwarze, K., Olendrowitz, C., Schoofs, L., Richmond, J., and Eimer, S. (2009). UNC-108/RAB-2 and its effector RIC-19 are involved in dense core vesicle maturation in Caenorhabditis elegans. J. Cell Biol. *186*, 897–914.

Tisdale, E.J., Bourne, J.R., Khosravi-Far, R., Der, C.J., and Balch, W.E. (1992). GTP-binding mutants of rab1 and rab2 are potent inhibitors of vesicular transport from the endoplasmic reticulum to the Golgi complex. J. Cell Biol. *119*, 749–761.

Wang, H., Jing, M., and Li, Y. (2018). Lighting up the brain: genetically encoded fluorescent sensors for imaging neurotransmitters and neuromodulators. Curr. Opin. Neurobiol. *50*, 171–178.

Wightman, R.M., Jankowski, J.A., Kennedy, R.T., Kawagoe, K.T., Schroeder, T.J., Leszczyszyn, D.J., Near, J.A., Diliberto, E.J., Jr., and Viveros, O.H. (1991). Temporally resolved catecholamine

spikes correspond to single vesicle release from individual chromaffin cells. Proc. Natl. Acad. Sci. U S A *88*, 10754–10758.

Wlodarska, M., Willing, B., Keeney, K.M., Menendez, A., Bergstrom, K.S., Gill, N., Russell, S.L., Vallance, B.A., and Finlay, B.B. (2011). Antibiotic treatment alters the colonic mucus layer and predisposes the host to exacerbated Citrobacter rodentium-induced colitis. Infect Immun. *79*, 1536–1545.

Zacharowski, K., Zacharowski, P.A., Koch, A., Baban, A., Tran, N., Berkels, R., Papewalis, C., Schulze-Osthoff, K., Knuefermann, P., Zahringer, U., et al. (2006). Toll-like receptor 4 plays a crucial role in the immune-adrenal response to systemic inflammatory response syndrome. Proc. Natl. Acad. Sci. U S A *103*, 6392–6397.

Zhang, Q., Pan, Y., Yan, R., Zeng, B., Wang, H., Zhang, X., Li, W., Wei, H., and Liu, Z. (2015). Commensal bacteria direct selective cargo sorting to promote symbiosis. Nat. Immunol. *16*, 918–926.

Zhang, Q., Pan, Y., Zeng, B., Zheng, X., Wang, H., Shen, X., Li, H., Jiang, Q., Zhao, J., Meng, Z.X., et al. (2019). Intestinal Lysozyme liberates Nod1 ligands from microbes to direct insulin trafficking in pancreatic beta cells. Cell Res. *29*, 516–532.

Zheng, P., Zeng, B., Zhou, C., Liu, M., Fang, Z., Xu, X., Zeng, L., Chen, J., Fan, S., Du, X., et al. (2016). Gut microbiome remodeling induces depressive-like behaviors through a pathway mediated by the host's metabolism. Mol. Psychiatry *21*, 786–796.

STAR★METHODS

KEY RESOURCES TABLE

REAGENT or RESOURCE	SOURCE	IDENTIFIER
Antibodies		
Rabbit Anti-Human Nod1 Polyclonal	Novus Biologicals	Cat# NB100-56878,RRID:AB_837807
Anti-Nod1 Antibody, Unconjugated	Cell Signaling Technology	Cat# 3545, RRID:AB_823443
RAB2 antibody	Proteintech	Cat# 15420-1-AP, RRID:AB_2176874
Anti-Rab2a	Zen BioScience	Cat# 200506
RAB10 antibody [4E2]	Abcam	Cat# ab104859, RRID:AB_10711207
Synaptophysin Polyclonal Antibody	Thermo Fisher Scientific	Cat# PA1-1043, RRID:AB_2199026
Anti-Chga	Novus Biologicals	Cat# NBP2-4476
Chromogranin A Antibody	Abcam	Cat# ab15160, RRID:AB_301704
Tyrosine Hydroxylase Antibody	Novus	Cat# NB300-110, RRID:AB_10002491
Anti-GAPDH	Immunoway	Cat# YT5052
Mouse Anti-β actin mAb antibody	ZSGB-BIO	Cat# TA-09, RRID:AB_2636897
Anti-Epinephrine	Abbexa	Cat# ABX100507
Goat anti-Rabbit IgG (H+L) Cross-Adsorbed Secondary Antibody, Alexa Fluor 555	Thermo Fisher Scientific	Cat# A-21428, RRID:AB_2535849
Goat anti-Mouse IgG (H+L) Cross-Adsorbed Secondary Antibody, Alexa Fluor 555	Thermo Fisher Scientific	Cat# A-21422, RRID:AB_2535844
Goat anti-Rabbit IgG (H+L) Cross-Adsorbed Secondary Antibody, Alexa Fluor 488	Thermo Fisher Scientific	Cat# A-11008, RRID:AB_143165
Goat anti-Mouse IgG (H+L) Cross-Adsorbed Secondary Antibody, Alexa Fluor 488	Thermo Fisher Scientific	Cat# A-11001, RRID:AB_2534069
Goat anti-Rat IgG (H+L) Cross-Adsorbed Secondary Antibody, Alexa Fluor 488	Thermo Fisher Scientific	Cat# A-11006, RRID:AB_2534074
Donkey anti-Sheep IgG (H+L) Cross-Adsorbed Secondary Antibody, Alexa Fluor 594	Thermo Fisher Scientific	Cat# A-11016, RRID:AB_2534083
Donkey Anti-Mouse IgG(H+L), CoraLite488 conjugate antibody	Proteintech	Cat# SA00013-5, RRID:AB_2890971
Mouse Anti-Rabbit IgG-HRP antibody	SouthernBiotech	Cat# 4090-05, RRID:AB_2650510
Goat anti-Mouse IgG (H+L) pAb-HRP	MBL	Cat# 330
Anti-GFP antibody	Roche	Cat# 11814460001, RRID:AB_390913
Anti-rabbit IgG (H+L), F(ab)2 Fragment (Alexa Fluor 647 Conjugate) antibody	Cell Signaling Technology	Cat# 4414, RRID:AB_10693544
Bacterial and virus strains		
Biological samples		
Chemicals, peptides, and recombinant proteins		
Normal goat serum blocking reagent	Boster Biotech	Cat# AR1009
DAPI	Novon	Cat# SS0156
Fluoromount-G	Southern Biotech	Cat# 0100-01
DAB Peroxidase (HRP) substrate	Maixin Biotech	Cat# DAB-0031
Hematoxylin solution	Sigma-Aldrich	Cat# 03971
PageRuler Prestained protein Ladder	Thermo Fisher	Cat# 26616
Pure nitrocellulose blotting membrane	PALL	Cat# P/N 66485

(*Continued on next page*)

Continued

REAGENT or RESOURCE	SOURCE	IDENTIFIER
Luminata Forte Western	Millipore	Cat# WBLUF0100
DMEM	Hyclone	Cat# sh3002201B
FBS	Bioind	Cat# 04-001-1A
RPMI 1640 Medium	Gibco	Cat# 11875-093
Endotoxin free PBS	Gibco	Cat# 10010-023
Lipofectamine 2000	Thermo Fisher	Cat# 11668019
Lipofectamine 3000	Thermo Fisher	Cat# L3000001
Hexadimethrine bromide (polybrene)	Sigma-Aldrich	Cat# H9268
Trizol	Thermo Fisher	Cat# 15596018
iE-DAP	InvivoGen	Cat# tlrl-dap
Muramyldipeptide (L-D isoform, active)	InvivoGen	Cat# tlrl-mdp
LPS-EB (LPS from E. coli O111:B4)	InvivoGen	Cat# L2630-100MG
iE-Lys	InvivoGen	Cat# tlrl-lys
PrimeScript RT reagent Kit	TAKARA	Cat# DRR047A
SYRB Premix Ex Taq	TAKARA	Cat# DRR820A
Leupeptin	Leagene Biotechnology	Cat# PI0029
Chloroquine diphosphate	Abcam	Cat# ab142116
Gentamicin sulfate salt	Sigma-Aldrich	E003632-1G
Vancomycin hydrochloride from Streptomyces orientalis	Sigma-Aldrich	V2002-100MG
Metronidazole	Sigma-Aldrich	M1547-5G
Neomycin trisulfate salt hydrate	Sigma-Aldrich	N6386-5G
Ampicillin sodium salt	Sigma-Aldrich	A9518-25G-9
Critical commercial assays		
Adrenaline Research ELISA	Labor Diagnostika Nord	Cat# BA E-5100
glycogen content assay kit	Solarbio	Cat# BC0340
UltraSensitive TM S-P Kit mouse	Maixin Biotech	Cat# KIT-9701
UltraSensitive TM S-P Kit rabbit	Maixin Biotech	Cat# KIT-9706
Experimental models: cell lines		
PC-12	China Infrastructure of Cell Line Resources	Cat# TCR 8
Experimental models: organisms/strains		
Mouse: *Nod1*$^{-/-}$	Our lab (Zhang et al., 2019)	N/A
Mouse: *Lyz1*$^{-/-}$	Our lab (Zhang et al., 2019)	N/A
Mouse: *Dbh-Cre*	MMRRC	RRID:MMRRC_036734-UCD
Mouse: *Nod1*$^{f/f}$	Our lab (Zhang et al., 2019)	N/A
Mouse: C57BL/6J	C57BL/6JTshu	N/A
Oligonucleotides		
PCR primers	This paper	See Table S1
Recombinant DNA		
pDisplay-NE1m-IRES-mCherry-CAAX	(Feng et al., 2019)	N/A
peGFP-C1	Addgene	Cat# 6084-1
Rab2a cDNA cloned from HEK-293T	This study	N/A

(*Continued on next page*)

Continued

REAGENT or RESOURCE	SOURCE	IDENTIFIER
Software and algorithms		
GraphPad Prism v8	GraphPad software	https://www.graphpad.com/scientificsoftware/prism
Image J v1.48	NIH	https://imagej.nih.gov/ij/
Zeiss Zen Imaging software (blue edition)	Zeiss	https://www.zeiss.com/microscopy/int/softwarecameras.html
Nikon-Elements Advanced Research	Nikon	www.microscope.healthcare.nikon.com
Fiji	NIH	https://fiji.sc/
Other		
Original western blot images	This paper	Mendeley Data, V1, https://doi.org/10.17632/px5wfcvwwb.1

RESOURCE AVAILABILITY

Lead contact

Further information and requests for resources and reagents should be directed to and will be fulfilled by the lead contact, Zhihua Liu (zhihualiu@mail.tsinghua.edu.cn).

Materials availability

This study did not generate new unique reagents.

Data and code availability

All data produced or analyzed for this study are included in the published article and its supplementary information files.

EXPERIMENTAL MODEL AND SUBJECT DETAILS

Mice

Lyz1$^{-/-}$, *Nod1*$^{-/-}$ and *Nod1*$^{f/f}$ mice (C57BL/6 background) were described previously (Zhang et al., 2019). The *Dbh-Cre* (Tg(Dbh-cre)KH212Gsat/Mmucd) mice were a gift from Professor Chen Zhan (NIBS) and were originally from the Mutant Mouse Resource & Research Center (MMRRC) (Gerfen et al., 2013). The *Dbh-cre* mice were further crossed with *Nod1*$^{f/f}$ to generate conditional knockout (*Dbh-cre;Nod1*$^{f/f}$) mice. 2-4-month-old gender-matched mice were used in this study unless noted otherwise. All mice were bred at 3-6 animals per cage in a 12/12 h light-dark cycle with *ad libitum* access to food and water at a controlled temperature (23°C $\pm$ 2°C). All specific pathogen-free (SPF) mice were bred and housed in an AAALAC (Association for Assessment and Accreditation of Laboratory Animal Care) accredited barrier facility in Tsinghua University. The animal experiments in the methods sections were carried out in accordance with Tsinghua University animal protocols (protocol number 20-LZH4), approved by Institutional Animal Care and Use Committee (IACUC). Mice were sacrificed by hypoxia via carbon dioxide inhalation followed by cervical dislocation in accordance with AAALAC guidelines immediately after the end of the intended experiments or at 8–10 am.

METHOD DETAILS

Plasmids

Human Rab2a cDNA was reverse-transcribed from mRNA prepared from HEK293T cells and inserted into peGFP-C1 vector. The dominant-negative (S20N) Rab2a mutant was generated by PCR-mediated mutagenesis. Sequences were confirmed by Sanger sequencing.

ABX treatments

ABX mice (male) were prepared according to the published procedure (Hill et al., 2010). Briefly, mice were subjected to oral gavage daily for 10 days with 300 μL of autoclaved water or autoclaved water

supplemented with ampicillin (1 mg/mL), gentamicin (1 mg/mL), metronidazole (1 mg/mL), neomycin (1 mg/mL), and vancomycin (0.5 mg/mL). Otherwise, mice had *ad libitum* access to autoclaved water. Fecal samples were collected at the end of the experiment and total DNA was extracted using QIAamp Fast DNA Stool Mini Kit. A short segment of the 16S rRNA gene was specifically amplified by real-time PCR using UniF340 (5′-ACTCCTACGGGAGGCAGCAGT-3′) and UniR514 (5′-ATTACCGCGGCTGCTG-GC-3′) to determine the total amount of commensal bacteria (Wlodarska et al., 2011).

Oral iE-DAP supplementation to mice

iE-DAP was dissolved in endotoxin-free PBS. 8-10-week-old male mice were gavaged with iE-DAP (1 mg/mouse) or PBS (mock) twice begin at 8 pm, 12 hr apart. 4 hours after the second gavage, mice were sacrificed and adrenal glands were collected for epinephrine measurement or *ex vivo* $GRAB_{NE}$ assay.

PC-12 cell culture, transfection, immunofluorescence staining and image quantification

PC-12 cells were obtained from China Infrastructure of Cell Line Resources (Cat# TCR 8) and verified based on their morphology under the microscope and by their growth curve. PC-12 cells were cultured in RPMI-1640 medium supplemented with 10% fetal bovine serum and 1% Pen/Strep. The cells were cultured at 37°C in a humidified atmosphere containing 5% CO_2. PC-12 cells in 24-well plates were transfected with 1 μg indicated plasmid and 3 μL Lipofectamine 2000 in 300 μL Opti-MEM media following the manufacturer's instruction. 24 hours post-transfection, transfected cells were treated with leupeptin (100 mM), chloroquine (50 mM) or DMSO (mock-treated) for another 24 hr in growth medium before being processed for immunofluorescence staining.

For immunofluorescence staining, cells grown on coverslips were washed with cold PBS and fixed in 4% PFA for 15 min at 4°C. Cells were then washed three times with PBS and blocked with antibody dilution buffer (PBS supplemented with 5% goat serum and 0.1% saponin) for 30 min. Cells were incubated with primary antibodies at 4°C overnight followed by fluorophore-conjugated secondary antibodies at RT for 2 hr. Samples were washed in PBS containing 0.1% Tween 20 three times between steps. Antibody dilution buffer was used throughout for antibody incubation steps. Coverslips were then counterstained and mounted onto slides in Fluoromount-G. Confocal images were obtained with a Nikon Ti confocal microscope under a 63× oil objective.

Fluorescence quantification of Chga staining was performed using a Nikon Ti NE imaging system. Cells were selected based on positive staining with anti-eGFP antibody and the boundary of the selected cell was drawn using ROI (region of interest) manager (Nikon-Elements Advanced Research Imaging Software). Fluorescence intensity of the individual selected cells was determined by Nikon-Elements Advanced Research Imaging Software. At least 988 GFP^+ cells (from more than 70 frames) were quantified per sample. Fluorescence intensity of Chga staining in cells transfected with Rab2a WT and S20N (Both eGFP positive and Anti eGFP positive) were calculated and analyzed. We then excluded the data of cells that fluorescence intensity of red channel was lower than 10^5 AU (mislabeled cell fragments) and higher than $2*10^7$ AU (abnormally high deviation values) in the statistical data.

Adrenal gland dissection and size analysis

WT, *Lyz1*$^{-/-}$, *Nod1*$^{-/-}$, *Dbh-cre;Nod1*$^{f/f}$, *Nod1*$^{f/f}$ and *Dbh-cre* mice (male) were anesthetized with CO_2, and the glands were dissected on ice and adipose tissue was removed. The isolated adrenal glands were weighed. Tissues were then immediately fixed in 4% PFA solution for 12 hr and finally embedded in paraffin and serially sectioned at 6 mm intervals. Images (every 10^{th} section) were captured with a 3DHISTECH panoramic system. In each image, the areas of the entire gland and the medulla were quantified using ImageJ. The sum of the areas of all sections was used to estimate total and medullary volumes in the glands from each genotype.

Isolation and culture of mouse adrenal chromaffin cells

Primary chromaffin cells were prepared from adrenal glands using the following procedure, as previously described by Aaron Kolski-Andreaco et al (Kolski-Andreaco et al., 2007). First, male mice were anesthetized with CO_2, and dissected adrenal glands were placed into a dish containing oxygenated Locke's buffer (NaCl 140 mM, KCl 5 mM, HEPES 10 mM, glucose 10 mM, $MgCl_2$ 1.2 mM, $CaCl_2$ 2.2 mM; pH 7.35, osmolarity between 295 and 300 mOsm) on ice, and cortexes were removed. Second, adrenal medullas were digested

for 25 min twice in DMEM with papain (40 unit/ml), 1 mM $CaCl_2$ and 0.5 mM EDTA at 37°C. Subsequently, the medullas were disrupted by pipetting gently in complete medium with DMEM, 5% fetal calf serum,10% horse serum, and 5 μL/mL penicillin and streptomycin. Cells were pelleted for 8 min at 200 g. Pellets were resuspended in complete medium and plated on poly-L-lysine-pretreated coverslips or in imaging chambers. Finally, primary adrenal chromaffin cells were then kept in an incubator at 37°C with 5% CO_2. Cell viability was determined by trypan blue staining, and cell preparations with >95% viability were used for further assays.

Amperometric recording and analysis

Isolated chromaffin cells were obtained from the adrenal glands of adult (11–13 weeks old) male WT, *Lyz1*$^{-/-}$ and *Nod1*$^{-/-}$ male mice. Amperometric recordings were performed after 1–3 days in culture at room temperature. The bath solution contained 140 mM NaCl, 2.7 mM KCl, 5 mM $CaCl_2$, 1 mM $MgCl_2$, 10 mM HEPES/NaOH, and 5–10 mM glucose. Osmolarity was around 300 mOsm, and the pH was adjusted to 7.3 with NaOH. To trigger secretion, KCl concentration was increased to 95 mM with a reduction of NaCl concentration to maintain the osmolarity. Chromaffin cells were stimulated by high potassium solution (95 mM KCl) contained in a puffing pipette located around 15 μm away from the recorded cell. The working potential of the carbon fiber electrode (CFE) was held at +700 mV with a patch-clamp amplifier (EPC10, HEKA, Germany). With a micromanipulator (MPC200, Sutter Instruments, USA), the CFE was slowly advanced to the chromaffin cell of interest.

The amperometric currents were recorded with sampling frequency 20 kHz and analyzed using the 'Quantal Analysis' program in Igor Pro (Version 6.2, WaveMetrics, Lake Oswego, USA), written by Drs. Mosharov and Sulzer (Mosharov and Sulzer, 2005). Data for offline analysis were low-pass-filtered at 1 kHz. A level of 5× the RMS of noise at baseline was set as the threshold for signal detection(Chen et al., 2021). Spike amplitude I_{max} is the spike maximum from the baseline current. The total charge during a spike event (Q) is calculated from the integral of the current (I) as $Q = \int I dt$. For the amount of catecholamine (N), the number of molecules is calculated as $N = Q/(n \times e)$, where n is the number of electrons donated by each catecholamine molecule (n=2 for catecholamine) and e is the elementary charge ($e = 1.6 \times 10^{-19}$). The two-tailed t test was used for statistical analysis. Error bars are standard error of the mean (s.e.m.).

Characterization of $GRAB_{NE}$ in PC-12 cells

Cultured PC-12 cells (6 cm dish) were transfected with 4 μg $GRAB_{NE}$ sensor, 10 μL P3000 and 10 μL Lipofectamine3000 in 300 μL Opti-MEM medium following the manufacturer's instructions. After 24 hr, the mixture of Opti-MEM-Lipofectamine-plasmid-medium was replaced again by complete medium. After another 12 hr, the cells were harvested and plated on cell coverslips. 24 hours later, iE-DAP (1 μg/mL), iE-Lys (1 μg/mL), MDP (1 μg/mL) or LPS (500 ng/mL) was added into the complete medium. After a further 6 hr, the fluorescence of $GRAB_{NE}$ sensor was imaged by Nikon Ti confocal microscope under a 63× oil objective for further analysis.

Ex vivo K^+-stimulated catecholamine secretion assay ($GRAB_{NE}$ assay)

Cultured primary chromaffin cells were transfected following a published procedure (Meunier et al., 2013). Briefly, primary chromaffin cells were plated into imaging chambers and allowed to adhere for 3 hr. Complete medium was replaced with Opti-MEM medium, and the cells were transfected with 1 μg $GRAB_{NE}$ using 2 μL Lipofectamine 2000. After 60 min, the mixture of Opti-MEM-Lipofectamine-plasmid was replaced again by complete medium to end the transfection procedure. The cells were used for the secretion assay 48 hr later. In the experiment with chromaffin cells from WT and *Nod1*$^{-/-}$ mice, iE-DAP (1 μg/mL), iE-Lys (1 μg/mL), MDP (1 μg/mL) or LPS (500 ng/mL) was added into the complete medium of 6 hr prior to the secretion $GRAB_{NE}$ assay.

For the secretion assay, chromaffin cells in the chamber were first bathed in Tyrode's solution (pH = 7.3–7.4) before KCl was added to reach a concentration of 90 mM. The fluorescence changes of recorded cells were imaged with an inverted Ti-E A1 confocal microscope with 525/50 and 600/30 nm emission filters to collect the green and red fluorescence, respectively. Individual cells were recorded for 5 min, with images taken every 5 s and the exposure time set at 50 ms per frame under the same microscopic parameters. The cell boundary was drawn using ROI manager, and fluorescence intensity value (FI) of individual cells were acquired. The instantaneous fluorescence change ΔF/F0 was calculated as (Ft - F0)/F0. The average at the five different time points before K^+ stimulation was defined as F0.

Extraction of adrenal glands

Whole adrenal glands from WT, *Lyz1*$^{-/-}$, *Nod1*$^{-/-}$, *Dbh-cre;Nod1*$^{f/f}$, *Nod1*$^{f/f}$ and ABX mice (male) were dissected on ice. Subsequently, the isolated adrenal glands were weighed and homogenized in acetonitrile (30 μL for every 1 mg of tissue). Ascorbic acid (final concentration at 3 mg/mL) was added as antioxidant. After thorough homogenization, samples were further sonicated for 60 s to fully extract catecholamines. The homogenates were centrifuged at 12,000 rpm for 10 min at 4°C. Supernatants were collected and stored at −80°C before quantification.

Immobilization and plasma preparation

Mice were subjected to restraint stress in a plastic piping bag (16*28*6.4 cm) for 25 min (for glycogen detection) or 1 hr (for epinephrine quantification) at 8 am. The tip (1 cm in length) was removed to allow airflow. During the restrain, animals could move their heads but were unable to move their limbs. For the control group, the mice were placed in their home cages at the same time without food and water.

At the end of the restraint, blood samples were collected into tubes containing 5 mM EDTA through orbital sinus bleeding. Subsequently, the plasma samples were prepared by centrifugation at 8000 rpm for 10 min at 4°C. The plasma samples were stored at −80°C before analysis.

Epinephrine quantification

The concentration of epinephrine in tissue or plasma samples was measured using an Adrenaline Research Elisa kit (BA E−5100) from Labor Diagnostika Nord (LDN) following the manufacturer's instruction.

Detection of glycogen

The amount of glycogen in liver was quantified using a glycogen content assay kit (Solarbio, BC0340, China) according to the manufacturer's instructions.

Immunofluorescence (IF) staining and immunohistochemistry staining of tissue sections

Murine tissues were fixed in 4% PFA/PBS overnight, dehydrated and embedded in paraffin. Tissue slices (6 μm in thickness) were mounted on positively charged glass and dewaxed. Antigen retrieval was performed by incubation in 0.01 M sodium citrate buffer (pH 6.0) for 25 min in a boiling steamer. For immunofluorescence staining, slides were then blocked with normal goat serum blocking reagent for 30 min, followed by sequential incubation with primary antibodies at 4°C overnight and fluorophore-conjugated secondary antibodies at RT for 2 hr. Slides were then counterstained with DAPI and mounted in Fluoromount-G. Confocal images were obtained with Zeiss LSM 710 or Nikon Ti NE imaging systems.

For IHC staining, slides were treated with an UltraSensitive TM S-P Kit after the antigen retrieval step. After sequential incubation with hydrogen peroxide (~15 min), blocking serum (~20 min), primary antibodies (overnight at 4°C), biotinylated secondary antibody (~20 min) and streptavidin-peroxidase (~20 min), immunoreactivity was visualized using diaminobenzidine (DAB). The slides were counterstained with hematoxylin, mounted, and observed with a light microscope (Nikon Eclipse 90i).

Image analysis and quantification

Quantitation of the fluorescence was performed using ImageJ as described by Shihan et al. (Shihan et al., 2021). Briefly, fluorescence images were captured on a Zeiss LSM 710 confocal microscope or Nikon Ti confocal microscope. Image analysis was performed using Fiji (an image processing package — a "batteries-included" distribution of ImageJ). Representative fluorescence images in each group were analyzed for quantification. Automatic thresholding was used to convert the image to a binary mask that included all fluorescence data above background. We calculated the mean intensity of fluorescence for each image and exported the data from Fiji into prism for further analysis and presentation.

Gene expression analysis using quantitative reverse-transcription PCR

RNA was extracted using Trizol from dissected adrenal medulla, dissected adrenal cortex, heart, brain, kidney, whole adrenal gland, spleen and lung (from male or female mice), and stored at −80°C. RNA was then quantified and purified with a PrimerScript RT reagent kit. q-PCR reactions were performed with SYBR Premix Taq on a Rotor Gene 6000 thermal cycler in triplicate. The following thermal cycling conditions were used: 95°C for 30 s, followed by 40 cycles of 95°C for 5 s and 60°C for 34 s. The specificity of q-PCR was

verified with melting curves for each PCR reaction. The level of target mRNA was determined by Delta-Delta Ct values between the target and loading control. Primers for q-PCR are listed in the Supplementary Information. Quantitative reverse-transcription PCR primers can be found in the Table S1.

Western blotting

The dissected adrenal medullas were homogenized in RIPA buffer (150 mM NaCl, 1% NP-40, 0.5% sodium deoxycholate, 0.1% SDS, 50 mM Tris pH 8.0, 5.0 mM EDTA pH 8.0, 0.5 mM dithiothreitol) supplemented with a protease inhibitor cocktail and 10 mM PMSF. The lysates were placed on ice for 30 min, then centrifuged at 12,000 rpm for 10 min. Tissue lysates were separated on SDS-PAGE gels and blotted onto immobilon-p PVDF membranes. After blocking in 5% skim milk in PBS-T (0.1% Tween 20) for 1 hr at room temperature, membranes were incubated with primary antibody at 4°C overnight and secondary HRP-conjugated antibodies and visualized by using ECL detection reagent. Protein band intensity was quantified using ImageJ software.

Electron microscopic analysis of DCGs in adrenal chromaffin cells

Isolated adrenal glands from euthanized mice were washed with cold PBS, and cortexes were removed in 0.1 M sodium phosphate buffer (pH 7.2) containing 2.5% glutaraldehyde and 2% paraformaldehyde. Adrenal medullas were then fixed in 0.1 M sodium phosphate buffer (pH 7.2) containing 2.5% glutaraldehyde and 2% paraformaldehyde at 4°C overnight. Dehydration was performed with an ethanol gradient followed by infiltration and embedding with an SPI-Pon 812 Epoxy Embedding Kit. Sections were cut on a Leica Ultracut Ultramicrotome (Leica EM UC6) and stained with uranyl acetate and lead citrate. The digital images were obtained using a transmission electron microscope (Hitichi H-7650) at 80 kV. Magnifications are indicated in the figure legend. Norepinephrine-storing cells were distinguished from epinephrine-storing cells based on the characteristics of the dense cores. Only epinephrine-storing cells were selected and analyzed in our study.

Image analysis were performed by a blinded researcher. The diameters of dense cores were measured using ImageJ software.

QUANTIFICATION AND STATISTICAL ANALYSIS

Statistical analysis was performed using GraphPad Prism 8.1. Student's *t*-test was used for comparisons between two groups. One-way ANOVA was used for comparisons between more than two groups. The respective statistical test used for each figure is noted in the corresponding figure legends and statistically significant differences are noted as ns ($p > 0.05$), *$p \leq 0.05$, **$p \leq 0.01$, ***$p \leq 0.001$, ****$p \leq 0.0001$. We summarized the statistical information in Table S2.